



Projected future changes in tropical cyclone-related wave climate in the North Atlantic

Ali Belmadani¹ · Alice Dalphiné² · Fabrice Chauvin³ · Romain Pilon^{1,4} · Philippe Palany¹

Received: 7 January 2020 / Accepted: 18 January 2021 / Published online: 8 February 2021
© The Author(s), under exclusive licence to Springer-Verlag GmbH, DE part of Springer Nature 2021

Abstract

Tropical cyclones are a major hazard for numerous countries surrounding the tropical-to-subtropical North Atlantic sub-basin including the Caribbean Sea and Gulf of Mexico. Their intense winds, which can exceed 300 km h^{-1} , can cause serious damage, particularly along coastlines where the combined action of waves, currents and low atmospheric pressure leads to storm surge and coastal flooding. This work presents future projections of North Atlantic tropical cyclone-related wave climate. A new configuration of the ARPEGE-Climat global atmospheric model on a stretched grid reaching $\sim 14 \text{ km}$ resolution to the north-east of the eastern Caribbean is able to reproduce the distribution of tropical cyclone winds, including Category 5 hurricanes. Historical (1984–2013, 5 members) and future (2051–2080, 5 members) simulations with the IPCC RCP8.5 scenario are used to drive the MFWAM (Météo-France Wave Action Model) spectral wave model over the Atlantic basin during the hurricane season. An intermediate 50-km resolution grid is used to propagate mid-latitude swells into a higher 10-km resolution grid over the tropical cyclone main development region. Wave model performance is evaluated over the historical period with the ERA5 reanalysis and satellite altimetry data. Future projections exhibit a modest but widespread reduction in seasonal mean wave heights in response to weakening subtropical anticyclone, yet marked increases in tropical cyclone-related wind sea and extreme wave heights within a large region extending from the African coasts to the North American continent.

1 Introduction

Tropical cyclones (hereafter TCs) are a major hazard for numerous countries surrounding the tropical-to-subtropical North Atlantic sub-basin including the Caribbean Sea and Gulf of Mexico. According to the World Meteorological Organization (WMO), they accounted for over half of all hydrometeorological and climate-related disasters reported

in North America, Central America and the Caribbean during recent decades, and for as much as 72% and 79% of the associated deaths and economic losses, respectively (WMO 2014). The Saffir-Simpson scale has been used since the 1970s to classify Atlantic TCs according to their intensity, estimated at any given time with their maximum 10-m sustained wind speeds, and is related to potential damage on infrastructure. Yet, it is now known that strong winds are responsible for < 10% of TC-related deaths in the United States, while nearly 90% are due to water-related incidents: storm surge (49%), heavy rain (27%), hazardous sea and surf in nearshore waters (6%) and further offshore (6%) (Rapport 2014). Thus about 6 fatalities out of 10 are induced by the marine response to TCs, where storm waves play a key role both directly and indirectly through their contribution to storm surge called wave set-up (e.g. Harris 1963; Komar 1998).

Further, wave run-up, which is the maximum height of instantaneous coastal water levels, is due to water intrusions over the swash zone and onto the beach slope induced by wave breaking and set-up (Stockdon et al. 2006, 2014). Particularly large run-ups caused by major hurricanes with wind

✉ Ali Belmadani
ali.belmadani@meteo.fr

¹ Direction Interrégionale Antilles-Guyane, Météo-France, Route du Général Brosset, Morne Desaix, BP645, Martinique, 97262 Fort-de-France Cedex, France
² Direction des Opérations, Prévision Marine, Météo-France, Toulouse, France
³ Centre National de Recherches Météorologiques, Météo-France/CNRS, Toulouse, France
⁴ Present Address: Laboratoire de Météorologie Dynamique, Institut Pierre-Simon Laplace, Sorbonne Université/CNRS/École Normale Supérieure-PSL Research University/École Polytechnique-IPP, Paris, France

speeds of up to 300 km h^{-1} or more can provoke coastal inundation and induce severe damage to coastal infrastructure and ecosystems (Rey et al. 2019). In a context of climate change associated with inevitable global-scale sea level rise (Church et al. 2013) and a possible increase in the frequency of major hurricanes (Christensen et al. 2013), adaptation measures along coastlines of the world ocean, and the North Atlantic in particular, therefore require an assessment of future projections of TC-related wave climate.

The number of studies dedicated to global and basin-scale wave climate projections has markedly increased over the last decade (Mori et al. 2010, 2013, Fan et al. 2013, 2014; Hemer et al. 2013a; Semedo et al. 2013, 2018; Wang et al. 2014, 2015; Guo et al. 2015; Shimura et al. 2015; Hemer and Trenham 2016; Camus et al. 2017; Kishimoto et al. 2017; Timmermans et al. 2017; Vousdoukas et al. 2018a, b; Webb et al. 2018; Morim et al. 2018), particularly in the framework of the Coordinated Ocean Wave Climate Project (COWCLIP, Hemer et al. 2014, 2018) WMO and Intergovernmental Oceanographic Commission (IOC) joint working group (Hemer et al. 2013b; Morim et al. 2019). The latter studies have compiled numerous individual studies to report robust future trends at the global scale across large community-based multimodel ensembles, and to quantify the associated uncertainties due to global climate model (GCM) wind forcing, wave modeling, and emission scenarios (Morim et al. 2019). While there is no doubt that such multimodel approaches provide invaluable information to decision makers as they significantly improve our confidence in wave climate projections, they also suffer from relatively coarse resolutions for modelled wave fields ($\sim 1^\circ$) and GCM wind forcings ($1\text{--}2^\circ$). This is a strong limitation for the assessment of TC-induced wave extremes (Wehner et al. 2015; Timmermans et al. 2017).

Indeed, while some GCMs exhibit weak TC-like vortices (Scoccimarro et al. 2011), resolutions of $35\text{--}50 \text{ km}$ are necessary to improve their representation, although with limited performance for major hurricanes (Chauvin et al. 2006; Julien et al. 2014). Recent research suggests that resolutions of 25 km and higher are needed to fully resolve the observed distribution of TC intensity (Wehner et al. 2015; Chauvin et al. 2020) and associated wave extremes (Timmermans et al. 2017). Therefore, while most of the aforementioned global- and basin-scale studies report on projected changes in extreme wave heights (e.g. Fan et al. 2013; Semedo et al. 2013; Guo et al. 2015), their conclusions remain questionable in TC regions.

A few exceptions include the 20-km and 25-km winds used by Mori et al. (2010) and Timmermans et al. (2017), respectively. The former study however used a rather coarse 1.25° wave model, which is also likely to bias TC wave extremes compared to the 25-km model implemented by Timmermans et al. (2017), as demonstrated by Chen et al.

(2018). The study by Timmermans et al. (2017), which represents the state of the art for global projections of TC-related wave climate, suggests possible large increases in extreme wave height in areas such as the tropical central and eastern North Pacific. Nevertheless, the patterns of expected future changes were noisy and clearly influenced by individual TCs, particularly in the Atlantic, because of the relatively short 23-year simulations, leaving the response of Atlantic TC wave climate to global warming as an open question. Alternative approaches include parametric TC winds (Krien et al. 2018, and references therein) that provide reasonably realistic and computationally cost-effective high-resolution forcing, combined with synthetic TCs statistically down-scaled from GCMs under various climate scenarios (e.g. Emanuel et al. 2013). However, the high-resolution wave models and associated computational burden remain limiting factors, restricting this approach to regional studies (Appendini et al. 2017).

Here we use ARPEGE-Climat, an atmospheric GCM with a stretched grid reaching 14 km resolution in the tropical North Atlantic (Chauvin et al. 2020). It forces a 10-km regional wave model, embedded into a 50-km wave model of the Atlantic Ocean, to infer projected future changes in North Atlantic TC-related wave climate. Unlike Timmermans et al. (2017), 30-year ensemble simulations generate a sufficient number of TCs to infer some robust changes in hurricane wave climate and extreme wave heights. In addition, dynamical downscaling is used to assess the sensitivity of our projections to resolution of winds and waves in the TC main development region (hereafter MDR).

The atmospheric GCM simulations are forced with sea surface temperature (SST) from a single IPCC (Intergovernmental Panel on Climate Change) CMIP5 (Coupled Model Intercomparison Project phase 5) coupled GCM under a single RCP8.5 greenhouse gas (GHG) emission scenario. Most projected changes in TC activity found in this model however tend to be consistent with previous studies (Chauvin et al. 2020). In particular: increased proportion and intensity of Category 4 and 5 hurricanes, reduced total TC numbers, and a slight shift of TC activity towards the mid-latitudes. Figure 1 illustrates the latter two as a reduction in the frequency of TC days over most of the North Atlantic including the Caribbean Sea and Gulf of Mexico, and an increase in the $40\text{--}50^\circ\text{N}$ band, although now regarded as barely significant after accounting for the multiple-testing problem (Online Resource 1, Sect. 1). It also exhibits a strong, robust increase in TC numbers around Cape Verde extending into the MDR, particularly at the hurricane season peak in September (not shown). This had not been reported before and has been attributed to expected changes in African easterly wave activity (Chauvin et al. 2020). Our results show that TC-related wave climate is sensitive to these

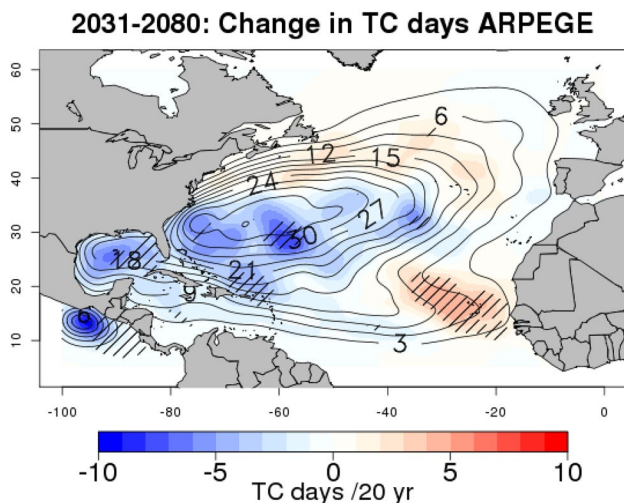


Fig. 1 Projected changes in the frequency of TC days between RCP8.5 (2031–2080) and Hist-Model (1965–2013). Values are expressed as a distance-weighted number of TC days per 20 years by $5^\circ \times 5^\circ$ square. Gaussian diffusion has been applied. Hist-Model frequency of TC days is overlaid as black contours. Hatchings are for the 5% significance level (Online Resource 1, Sect. 1). Adapted with permission from Chauvin et al. (2020)

projected changes in TC activity, both in the MDR and the extratropics.

The present paper is organized as follows. The model and observed datasets and the methodology are detailed in Sect. 2. The results for model evaluation against historical data and for projected future changes in seasonal mean, TC-mean and extreme wave climate are presented in Sect. 3. Section 4 is a discussion of the limitations of our study. Finally, concluding remarks are drawn in Sect. 5.

2 Data and methods

2.1 Model and observed data

2.1.1 ARPEGE-climat atmospheric general circulation model

Wind fields from a high-resolution atmospheric GCM are used to drive a wave model of the Atlantic basin and a nested high-resolution model of the MDR. The GCM is ARPEGE-Climat (Batté and Déqué 2016), the atmospheric component of the CNRM-CM CMIP coupled GCM developed at Météo-France, the French national weather service. ARPEGE-Climat offers the capability of a stretched grid, increasing the resolution over a given region at the computational cost of a standard coarse-resolution GCM, thanks to degraded resolution over the antipodes. In addition to numerous climate studies, it has been combined

with ocean wave models to perform wave climate projections around France on a 60–80 km stretched grid (Charles et al. 2012) and on a uniform 50 km grid (Laugel et al. 2014). Its CMIP5 coupled coarse-resolution configuration (1.4°), CNRM-CM5, was among the GCMs used in the multimodel wave climate projection studies by Wang et al. (2014), Hemer and Trenham (2016), Camus et al. (2017), and Morim et al. (2019).

Here we use a new configuration of ARPEGE-Climat that is being used for CMIP6 within the CNRM-CM6 coupled GCM (Voltaire et al. 2019; Roehrig et al. 2020), except for a stretched grid reaching ~ 14 km resolution to the north-east of the Lesser Antilles (Cantet et al. 2020). The model, its configuration and the associated climate simulations have been described in detail by Chauvin et al. (2020), so only a brief description is provided here.

ARPEGE-Climat has been forced with monthly SSTs from CNRM-CM5 under historical and RCP8.5 climates. SSTs from the historical simulations over 1965–2013 (hereafter Hist-Model) were previously corrected with HadISST1 observed monthly SSTs (Rayner et al. 2003) to ensure unbiased mean climatology, while the same correction was applied to SSTs from RCP8.5 simulations over 2031–2080 for consistency. ARPEGE-Climat has also been forced with HadISST1 SSTs over 1965–2014 (hereafter Hist-Obs) for the purpose of model comparison with observations. For each of these three climate experiments, 5 ensemble members differing only by their initial conditions allow reaching robust statistics regarding TC-related extremes (Chauvin et al. 2020). Thanks to high resolution, the model is able to represent the distribution of TC winds fairly well, including Category 5 hurricanes (Chauvin et al. 2020).

Six-hourly 10-m winds from the climate experiments (Hist-Obs, Hist-Model, and RCP8.5) with five members each (15 simulations in total) were interpolated onto regular 10-km and 50-km grids over the MDR and whole Atlantic Ocean, respectively, to drive ocean wave models (Sect. 2.1.2). Such forcing, as well as wind field analysis were considered over the reduced 1984–2013 (Hist-Obs, Hist-Model) and 2051–2080 (RCP8.5) periods (see details in Sect. 2.1.2). Winds at different vertical levels and other atmospheric variables were also interpolated onto a 15-km grid over most of the North Atlantic for the full fifty-to-sixty-year time slices in order to apply an automated TC tracking algorithm (Chauvin et al. 2020). The results have been used by Chauvin et al. (2020) to provide TC counts and climatology, as well as related projected future changes. We use some of that information (over the reduced 30-year periods) to define the hurricane season (Sect. 2.2.1) and extract TC-related wave climate (Sect. 2.2.2) and extreme wave heights (Sect. 2.2.3). The ARPEGE-Climat experimental setup and grid characteristics are summarized in Tables 1 and 2, respectively.

2.1.2 MFWAM spectral wave model

We make use of the MFWAM (Météo-France Wave Action Model) spectral wave model, a version of the WAM (WAMDI Group 1988) developed at Météo-France. MFWAM is a third generation wave model that computes the evolution of sea state in the spectral space thanks to the energy balance equation. It uses the ECWAM-IFS-38R2 code with a dissipation term developed by Ardhuin et al. (2010) and upgraded for the Copernicus Marine Environment Monitoring Service (CMEMS). This term involves the computation of the wave-supported stress from the model spectrum, which is used to modify wind friction velocity and ultimately wind stress through the wave-supported stress effect on sea surface roughness. Such parameterization reduces the drag coefficient and wind input for high wind speeds (Ardhuin et al. 2010), which is relevant for TCs because wave growth would otherwise be overestimated (Powell et al. 2003). The wave spectrum is discretized in 24 directions and 30 frequencies, from 0.035 Hz to 0.58 Hz (1300–5 m wavelengths).

The model applies watershed partitioning to split the wave spectrum into wind sea and various swell components. In the first step, the part of the wave spectrum where wind speed exceeds phase speed and wave propagation is aligned with surface winds is considered wind sea. A cosine factor is used to treat neighboring wave directions. The swell part is then partitioned to retrieve sea states of various origins. According to Hasselmann et al. (1996), wave spectra may be considered inverted catchment areas, allowing the use of hydrological methods like the watershed algorithm. Each secondary maximum in the direction-frequency spectrum

is thus considered a separate sea state. The most energetic is named primary swell, the second is secondary swell, and so on.

Several MFWAM configurations run every day at Météo-France. They are used to issue high surf advisories, watches and warnings for the open ocean and coastal areas. The MFWAM global configuration is also dedicated to CMEMS wave products (Aouf 2018).

Our configuration is derived from an operational setup with a 10-km regional grid for the Lesser Antilles and French Guiana (hereafter MFWAM01) nested in a 50-km global grid (MFWAM05). To reduce the computational burden associated with long ensemble simulations, and recognizing that distant swells from other basins have little influence on North Atlantic sea states (Alves 2006; Semedo et al. 2011), the MFWAM05 domain was restricted to the Atlantic (59.5°S–0°N, 99°W–21°E). The South Atlantic was included to allow the propagation of Southern Hemisphere swells into the North Atlantic, particularly in its eastern part as inferred from comparison to an experiment with the model southern boundary located at 10°S (not shown). We however excluded the latitudes north of 70°N where local swells are unlikely to influence lower latitudes in any significant way. For simplicity, sea ice was not taken into account. Although not global, the MFWAM05 configuration was only forced at the surface with ARPEGE-Climat winds without any prescribed wave spectra along the open boundaries.

The MFWAM01 domain was extended eastwards to make the most of highest-resolution MDR winds (5°N–28°N, 75°W–10°W). Three-hourly MFWAM05 spectra were prescribed at the open boundaries for remote swell propagation into the MFWAM01 domain. MFWAM01 wave spectra were

Table 1 Summary of the ARPEGE-Climat simulations used to drive the wave models

Climate experiment	Monthly SST forcing	Time slice (Chauvin et al. 2020)	Time slice (this study)	Number of ensemble members
Hist-Obs	HadISST1	1965–2014	1984–2013	5
Hist-Model	CNRM-CM5, historical, corrected	1965–2013	1984–2013	5
RCP8.5	CNRM-CM5, RCP8.5, corrected	2031–2080	2051–2080	5

Table 2 Summary of the horizontal grids considered for ARPEGE-Climat and for the MFWAM nested domains

Numerical model	Geographical domain	Horizontal resolution	Boundary forcing
ARPEGE-Climat	Global	Variable (Chauvin et al. 2020, their Fig. 1) Atlantic: TC regions 14–30 km (Gulf of Mexico ~ 35 km), subpolar regions 30–60 km, South Atlantic 30–100 km	None
MFWAM05	Atlantic 59.5°S–70°N/99°W–21°E	50 km	None
MFWAM01	MDR 5°N–28°N/75°W–10°W	10 km	MFWAM05 3-h wave spectra

however not fed back into the MFWAM05 domain (one-way nesting). Our purpose is to assess the sensitivity of our results to the resolution of winds and waves (in the MDR), rather than upscaling effects from the MDR to basin scale, which would require 2-way nesting. Table 2 summarizes the MFWAM nested grid configuration.

Since our focus is on TC-related wave climate, and given the high computational costs of dynamic wave model simulations for the whole calendar year over fifty-to-sixty-year periods with available ensemble wind data, temporal and seasonal subsampling had instead to be applied. For each climate experiment and ensemble member (Table 1), only the last 30 years were considered. This is a trade-off between numerical cost and periods long enough to minimize natural low-frequency variations, thus isolating the anthropogenic global warming signal. For RCP8.5 wave simulations (hereafter W-RCP8.5), we focus on long-term projections after the mid-21st century (2051–2080) and thus on the potentially largest changes. For W-Hist-Model and W-Hist-Obs simulations forced with Hist-Model and Hist-Obs winds (1984–2013), the pre-satellite era (before 1979) is excluded, guaranteeing observations of the highest possible quality for model calibration and validation (see Sect. 3.1). In addition, only the hurricane season (about 4 months from July to November, see Sect. 2.2.1) was simulated each year for the 15 available ARPEGE-Climat simulations (Table 1). Therefore, 450 simulations were run for MFWAM05 and MFWAM01. The analysis considers three-hourly outputs for significant wave height H_s , mean wave period T_m , and H_s partitioning into wind sea and primary swell (H_{s0} and H_{s1} , respectively). Table 3 summarizes the MFWAM experimental setup.

2.1.3 Reanalysis and altimetry wind and wave data

The European Centre for Medium-Range Weather Forecasts (ECMWF) ERA5 reanalysis (Hersbach et al. 2020) is used as a reference to assess surface winds in the ARPEGE-Climat Hist-Obs runs over the North Atlantic. Specifically, 6-h 10-m winds (interpolated at 0.5° resolution) over the 1984–2013 hurricane seasons (July 9 to November 9, see Sect. 2.2.1) and their standard deviation

are compared to those from the 5-member GCM archive (Table 1).

ERA5 features an ocean wave component coupled with the atmospheric reanalysis called ECWAM (European Centre Wave Action Model), which is the ECMWF version of WAM with a dynamical core similar to MFWAM. Similarly to surface winds, 6-hourly outputs are interpolated at 0.5° resolution. They are used to assess the MFWAM05 and MFWAM01 model performance in terms of mean H_s and T_m as well as their standard deviation. On the other hand, the older ERA-Interim reanalysis (Dee et al. 2011) was used to calibrate MFWAM in terms of the wave growth coefficient β_{max} to minimize model bias (see Sect. 3.1.2). ERA5 could not be used because the data was not yet available over the entire 1984–2013 period when the MFWAM simulations were performed. However, our calibration appears reasonable in the light of the comparison of model bias relative to ERA5 and altimetry data (Sect. 3.1.2).

To assess the uncertainty in observed wave climate, MFWAM mean H_s and its standard deviation were also compared to those from the remotely-sensed ESA CCI (European Space Agency Climate Change Initiative) Sea State 1° monthly level-4 multimission product version 1.1 (Piolle et al. 2020 ; Dodet et al. 2020). The comparison was performed over the available 1991–2013 record and the months of August to October (ASO). This is the longest sequence of complete months within the W-Hist-Obs hurricane season. The base data are the median H_s values over each satellite track portion, within each 1° bin over a one-month period. They are hereafter referred as h_{mp} ($p = 1, \dots, n_m$), where n_m is the number of such values for each month m . Various statistics particularly suitable for wave climate studies are provided (Timmermans et al. 2020; Dodet et al. 2020). ASO mean significant wave height $\overline{H_s}$ was estimated by ensemble-averaging the 69 available monthly averages of h_{mp} . For each month m , the sum of squared h_{mp} and n_m are also available. The ASO standard deviation of H_s over 1991–2013 was then estimated as:

Table 3 Summary of the MFWAM wave climate simulations

Climate experiment	6-h ARPEGE-climat wind forcing	30-year time slice	Period simulated each year	Number of ensemble members	Number of simulated hurricane seasons
W-Hist-Obs	Hist-Obs	1984–2013	July 9–November 9	5	150
W-Hist-Model	Hist-Model	1984–2013	July 6–November 10	5	150
W-RCP8.5	RCP8.5	2051–2080	July 20–November 3	5	150

The information provided applies to both MFWAM05 and MFWAM01

$$\sigma = \sqrt{\frac{1}{N} \sum_{m=1}^{69} \sum_{p=1}^{n_m} h_{mp}^2 - \overline{H_s}^2}, \quad (1)$$

where $N = \sum_{m=1}^{69} n_m$ is the total number of median H_s values over the entire period.

2.2 Methods

In this section, the methodologies used to estimate the hurricane season dates and to extract mean and extreme TC wave climate are presented. The statistical methods used to assess sampling uncertainties in our projections are detailed in the Online Resource 1.

2.2.1 Estimation of the hurricane season

According to WMO, the Atlantic hurricane season officially extends from June 1 to November 30. Yet, it was not necessarily appropriate to consider these dates. Indeed, our projections of TC-related wave climate are driven by climate models that are not able to reproduce the exact dates of the hurricane season. In addition, shifts in the season dates are expected (see Sect. 3.2). Since statistics over the W-Hist-Model and W-RCP8.5 hurricane seasons are compared, it requires independent definitions for historical and future seasons. Last, for matters of computational cost, a less conservative definition was sought to reduce season length. The use of fixed, standard dates may however be useful for matters of reproducibility (Sect. 4.6).

For each climate experiment (Hist-Obs, Hist-Model, RCP8.5), the hurricane season was defined as the period of the year when at least 30 so-called TC days were found for each calendar day among the 150-year multimember archive (Table 3). A given date is a TC day if at least one TC was detected in the North Atlantic sub-basin with the methodology of Chauvin et al. (2020). Therefore, the hurricane season is the time of the year with TC daily return period below 5 years.

Projected changes in extreme TC-related wave heights over the season peak when TC activity is highest are also of interest. Unlike the previous approach based on TC track data, we focus here on return periods of extreme wave heights directly as diagnosed from MFWAM01. To provide meaningful results in terms of potential impacts on coastal human settlements and ecosystems, the analysis is restricted to a region around the Lesser Antilles in the eastern Caribbean. Indeed, these small islands are the first landmasses crossing the path of TCs generated in the MDR.

Let $p(H_{S_{\max}} \geq 3 \text{ m})$ be the occurrence probability that the MFWAM01 maximum H_s over the eastern Caribbean (11.7–19°N, 59–64°W) exceeds 3 m for any given calendar 3-h time step among the 30-year, 5-member archive. The hurricane season peak was then arbitrarily defined as

the period when $p(H_{S_{\max}} \geq 3 \text{ m}) \geq 4.5\%$ (on average every 1.35 years out of 30). It is thus the time of the year with 3-h return period of these extreme events below ~22 years. Thresholds of 2 m and 4 m captured events that were respectively too frequent—thus neither extreme nor necessarily TC-related—and too rare, leading to noisy and not robust results (not shown).

2.2.2 Estimation of TC-related wave climate

One question addressed here is how the contribution to mean ocean wave climate of all TCs taken together (from tropical storms to major hurricanes), hereafter referred to as TC-related wave climate, is likely to change under a RCP8.5 scenario. Therefore, one needs to estimate TC-related wave climate in W-Hist-Model and W-RCP8.5. For a given parameter (H_s , H_{s0} , H_{s1} , T_m), the first step is to compute a composite average over all the TC days identified in the 150 model runs for each experiment (Table 3). More accurately, the average is computed over all the 3-h outputs included within TC days: 58,845 and 52,861 time steps in total for the 5 members of W-Hist-Model and W-RCP8.5, respectively. This is performed at every grid point with all time steps weighted equally.

However, this is not representative of mean TC-related wave climate because on any given TC day, TC conditions will only dominate over a fraction of the sub-basin. Sea states in other regions may be influenced by various drivers such as remote swells of extratropical origin, trade wind swells, local wind sea etc. In fact, composite averages appear similar to seasonal means because TCs are sufficiently rare at any given location for their average contribution to be minor. To reveal it, one thus needs to remove the hurricane-season mean field (i.e. averaged over both TC and non-TC days from the 150 simulated seasons) from the composite field (averaged over TC days only). It is assumed that other wave drivers are mostly uncorrelated with TCs and therefore not much different on average on TC and non-TC days. The derived anomalous field then represents TC-related wave climate, and the difference between the corresponding W-RCP8.5 and W-Hist-Model fields represents its future evolution.

2.2.3 Estimation of extreme TC-related wave heights

In addition to the contribution of all TCs to ocean wave climate, the wave response to expected changes in extreme TCs is also of interest. While many extreme wave height events during the hurricane season are induced by TCs, mid-latitude swells may also drive large waves, especially towards the season end (October and November) that coincides with autumn and seasonal increases in the frequency and strength

of mid-latitude low-pressure systems. To filter out such non TC-related wave extremes, only TC days are considered.

Following Wang et al. (2014), extreme TC-related H_s are estimated according to extreme value analysis. Independent and identically distributed realizations, which are necessary to compute unbiased statistics (Online Resource 1, Sect. 4), are obtained by only retaining the annual maximum value of H_s over TC days for each model grid point. In the rare cases with no TC days for a given year and ensemble member, which only occurred when the computation was restricted to the hurricane season peak (Sect. 3.2.3), the annual maximum H_s is taken over non-TC days (4 and 2 instances out of 150 for W-Hist-Model and W-RCP8.5, respectively). A Generalized Extreme Value (GEV) distribution is then fit to the resulting 150-value sample (Table 3) at each grid point, from which a 10-year return level and its associated 95% confidence interval are derived. As detailed in the Online Resource 1 (Sect. 4), the statistical significance of the associated projected changes is assessed considering any overlap between the confidence intervals from W-Hist-Model and W-RCP8.5.

3 Results

3.1 Atmospheric and wave model performance

3.1.1 ARPEGE-climat model performance

ARPEGE-Climat TC track analysis (see Sect. 2.2.1) yields the following model hurricane season dates: July 9 to November 9, July 6 to November 10, and July 20 to November 3 for Hist-Obs, Hist-Model, and RCP8.5, respectively (Fig. 2). Repeating with IBTrACS best-track data (Knapp et al. 2010) over 1984–2013 yields a season extending from July 5 to November 13. Hist-Obs and Hist-Model thus represent the hurricane season timing fairly well. ARPEGE-Climat however underestimates the number of TC days during the hurricane season, particularly around the season peak early September, while overestimating it off season (see also Chauvin et al. 2020; Cantet et al. 2020).

We then assess patterns of mean present-climate hurricane-season wind forcing using ERA5 as a reference. Hist-Obs features realistic low-level circulation compared to reanalysis data (Fig. 3a, b). The subtropical anticyclone is however weaker with a systematic bias of $\sim -1 \text{ m s}^{-1}$ (Fig. S2), which possibly results from the lack of data assimilation in the GCM. In contrast, surface wind standard deviation is overestimated by 20–30% across the sub-basin, particularly between the US East Coast and the Azores Islands (Fig. 3c). On the other hand, a slight underestimation (5–10%) is visible near 5–10°N between Africa and the Lesser Antilles. In fact, the standard deviation bias pattern appears quite similar

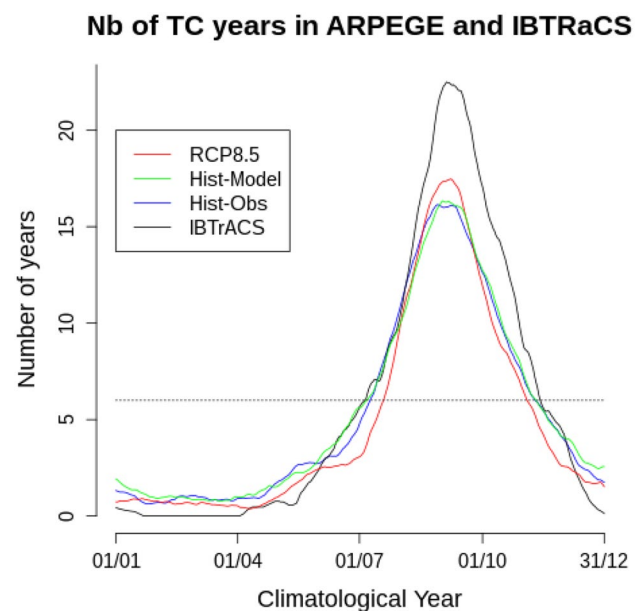


Fig. 2 Ensemble mean number of years with a TC day for each calendar day from RCP8.5 (2051–2080, red), Hist-Model (1984–2013, green), Hist-Obs (1984–2013, blue), and IBTrACS (1984–2013, black). The horizontal dotted line indicates the threshold used to define the hurricane season (6 years out of 30 i.e. every 5 years). A 30-day moving average was applied to filter out high-frequency noise

to present-climate frequency of TC days (black contours on Fig. 1), suggesting it may result from large TC activity in the subtropics compared to ERA5. Indeed, this is consistent with more TCs in the extratropics and less in the MDR compared to best-track data (Chauvin et al. 2020). Such data is however subject to some uncertainty (Knapp et al. 2010) and the relatively low-resolution reanalysis (native resolution is $\sim 30 \text{ km}$) cannot adequately grasp TC wind speeds, which may explain part of the model bias in the standard deviation. The secondary maximum at 15–20°N in standard deviation bias (Fig. 3c) may result from very strong TC winds compensating underestimated MDR TC numbers (Chauvin et al. 2020). Noteworthy, the comparison of ERA5 and Hist-Model (instead of Hist-Obs) yields almost identical bias in mean winds and their standard deviation (not shown).

3.1.2 MFWAM model performance

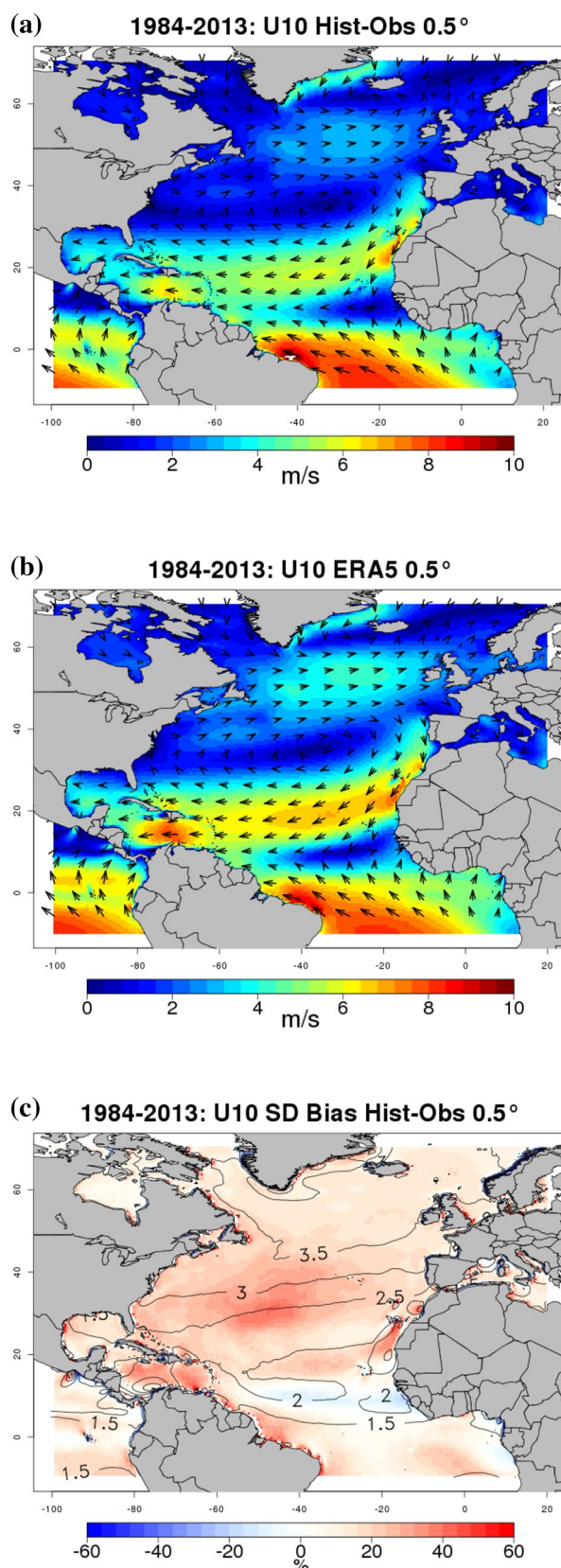
More frequent TCs and associated strong winds in the GCM subtropics than in reality trigger overly large waves and long-period swells in MFWAM05. Indeed, extratropical H_s and T_m were initially overestimated in a single-member set of W-Hist-Obs simulations by as much as +0.5–1 m and +1–1.5 s relative to ERA5, respectively (not shown). To compensate for the excessive wind variability, the wave growth coefficient β_{max} was reduced for both MFWAM05 and MFWAM01 after succinct calibration/validation against

Fig. 3 **a, b** Mean present-climate (1984–2013) hurricane-season surface winds (arrows) and wind speed U_{10} (shading, m s^{-1}) in **a**) Hist-Obs and **b**) ERA5. **c** Relative differences in the standard deviation of present-climate hurricane-season U_{10} between Hist-Obs and ERA5 (shading, %), with ERA5 values overlaid as black contours (m s^{-1}). All the data have been interpolated onto a 0.5° grid and are masked over land

ERA-Interim from 1.52 (operational configuration) to the value of 1.13 also used by Stopa (2018). Positive H_s and T_m biases were thereby reduced almost everywhere and particularly in the extratropics. It appeared difficult to reduce such biases ($\sim +0.4$ m and $\sim +0.5$ s, Fig. 4a, b) any further because of negative H_s bias of similar intensity in the tropics (Fig. 4a).

The comparison of model H_s with altimetry allows us to qualify these results to some extent. Despite the gridded ESA Sea State CCI data being only available over the reduced 23-year record and shorter ASO period shared with the wave model, the associated H_s bias pattern is similar (Fig. S3a). Compared with ERA5, the ESA Sea State CCI mean H_s is larger, consistently with Timmermans et al. (2020) and Dodet et al. (2020). As a result, the MFWAM05 positive (negative) bias in the subtropics (tropics) is reduced (slightly enhanced) when referred to ESA Sea State CCI. Although ESA Sea State CCI level-4 data is gridded at 1° , it is mostly a collection of 1-Hz alongtrack measurements with careful quality control and extensive calibration against wave buoys. As such, it is considered at least as reliable as ERA5 H_s data, which underestimate buoy observations at various locations including the northwestern Atlantic (Timmermans et al. 2020). Overall ERA-Interim appears as a reasonable choice for MFWAM05 calibration, other datasets revealing that biases are modest in H_s , although significant in T_m .

After calibration, the pattern of MFWAM05 H_s standard deviation is reasonable, featuring a marked increase with latitude similarly to mean H_s (not shown). However, H_s standard deviation is also overestimated in the extratropics by as much as 50–60% compared to ERA5. This most likely results from the overestimated wind variability, judging from the striking similarity in the respective bias patterns. See for example the positive and negative biases near $30\text{--}40^\circ\text{N}/40\text{--}50^\circ\text{W}$ and $5\text{--}10^\circ\text{N}/15\text{--}50^\circ\text{W}$, respectively (Figs. 3c, 4c). Satellite estimates confirm the excessive extratropical H_s variability though with weaker bias, while weak negative biases are found over the tropics and high latitudes (Fig. S3b). More variable mid-latitude wave heights than in the real ocean induce more variable swell periods in the tropics and along the sub-basin boundaries by up to 50% (Fig. 4d). Noteworthy, the overestimated T_m variability tends to concentrate in the MDR and along the US East Coast, right around the model TC region (Fig. 1). Overall, these findings suggest that our calibration, which is driven by a reduction in mean biases, does not necessarily



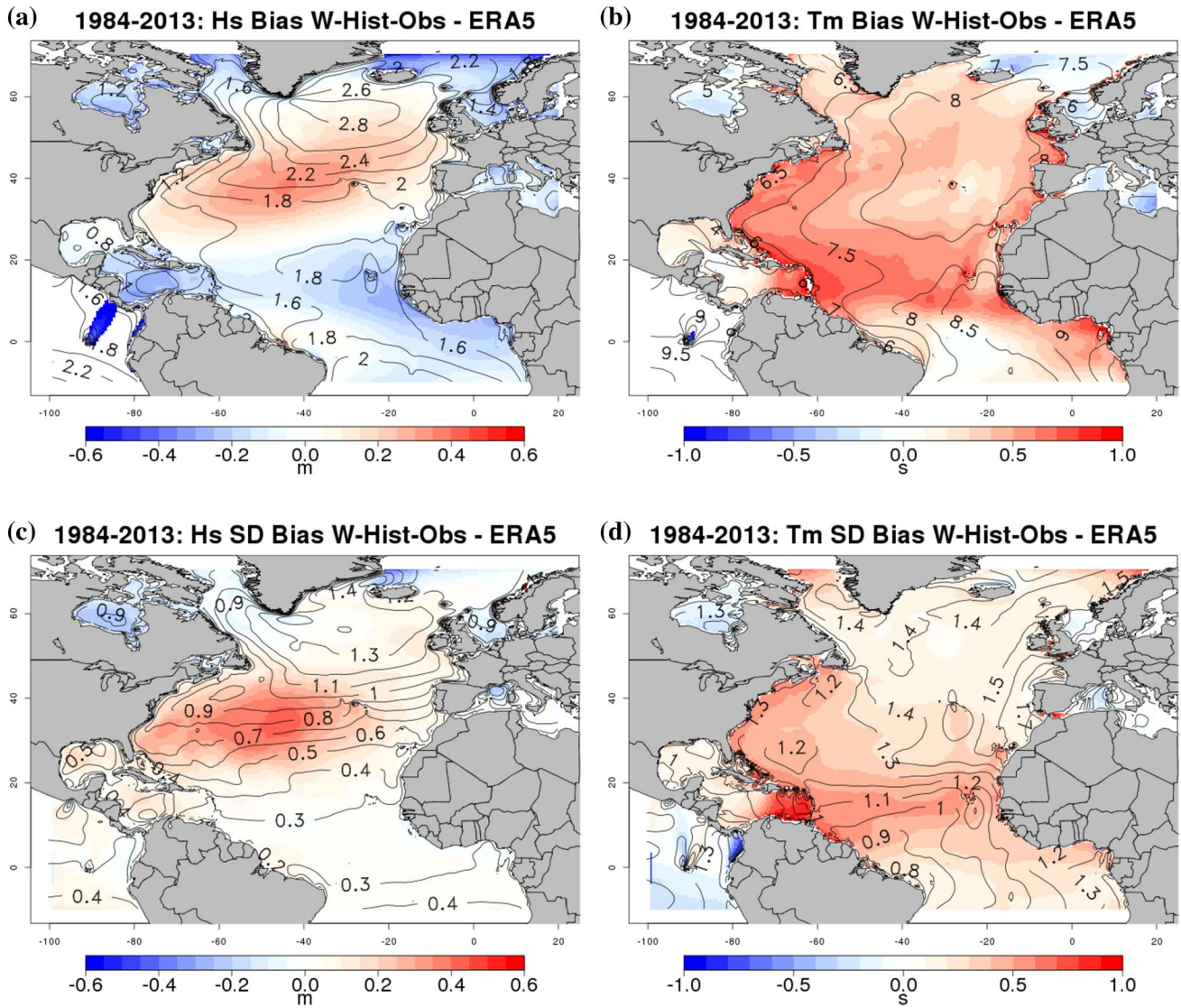


Fig. 4 Differences in the (a, b) mean and (c, d) standard deviation of present-climate (1984–2013) hurricane-season (a, c) significant wave height H_s (m) and (b, d) mean wave period T_m (s) between

MFWAM05 W-Hist-Obs and ERA5 (shading), with ERA5 values overlaid as black contours. The ERA5 data have been interpolated onto a 0.5° grid. Differences exceeding ± 0.6 m or ± 1.0 s are masked

lead to systematic overestimation of sea state variability (and possibly of extreme wave heights).

3.2 Projected future changes

3.2.1 Seasonal mean wave climate

First of all, one may note a slight shortening of the hurricane season that starts two weeks later and ends one week earlier in the future projections (Fig. 2). In ARPEGE-Climat under RCP8.5, trade winds and westerlies slow down by $0.5\text{--}1.5\text{ m s}^{-1}$, as shown on Fig. 5a by blue shading together with westerly and easterly wind vector anomalies near 10°N and 50°N , respectively. These differences in U_{10} between the

two ensembles are significant at the 5% level, as indicated by hatchings over most of the sub-basin. Such weakening of the subtropical anticyclone is accompanied by slight poleward migration of low-level circulation: zonal bands of positive wind speed anomalies in the subtropics and high latitudes are found to the north of the weakening easterly trade winds and westerlies, respectively. This is consistent with previously reported poleward widening and weakening Hadley cell with global warming (Johanson and Fu 2009; Gastineau et al. 2009), and specifically, decreasing wind speeds in the North Atlantic mid-latitudes (Kar-Man Chang 2018).

Weaker future winds trigger moderate yet robust 5–10% sub-basin-wide reduction in H_s , particularly in the mid-to-high latitudes and east of the Lesser Antilles (Fig. 5b), in

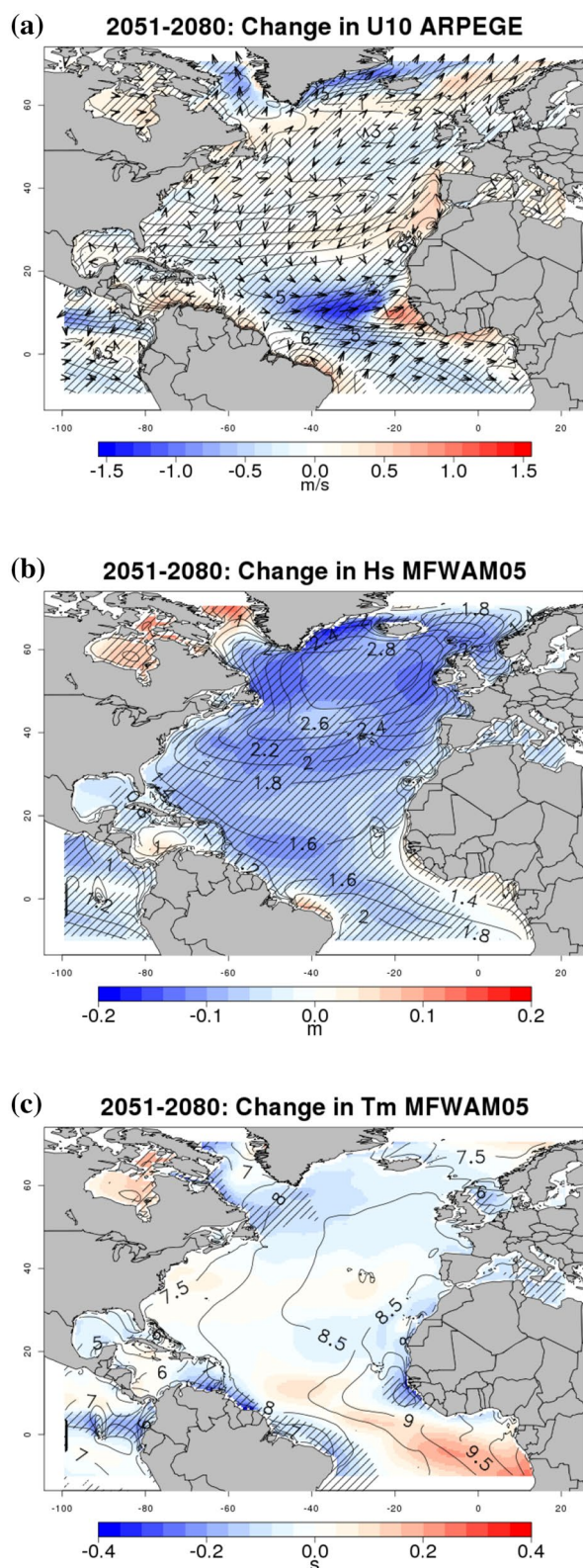
Fig. 5 Projected changes in hurricane-season mean **a** surface winds (arrows) and wind speed U_{10} (shading, m s^{-1}) from ARPEGE-Climat, **b** significant wave height H_s (m) and **c** mean wave period T_m (s) from MFWAM05 between W-RCP8.5 (2051–2080) and W-Hist-Model (1984–2013). W-Hist-Model values for U_{10} , H_s , and T_m are overlaid as black contours. Hatchings are for the 5% significance level (Online Resource 1, Sect. 2). ARPEGE-Climat data are masked over land. The arrows on **a** are for the difference between W-RCP8.5 and W-Hist-Model wind vectors

general agreement with CMIP3 and CMIP5 multimodel studies (Hemer et al. 2013b; Morim et al. 2019). Conversely, projected changes in T_m are weak over most of the sub-basin, except for a significant reduction along numerous coastal regions across the North Atlantic (Fig. 5c), possibly in response to weaker distant swells in W-RCP8.5.

The reduction in H_s extends over the entire hurricane season (Fig. 6a–c). It is however smallest and not statistically significant in late August and September, both in the mid-latitudes (Fig. 6a) and tropics (Fig. 6b, c). The reduction in mean H_s may be partly compensated by maximum increases in TC-related extreme wave heights at the hurricane season peak (see Sect. 3.2.3). Downward trends in mean H_s are evident in the mid-latitudes, ~ -1 cm/decade and ~ -2.5 cm/decade for W-Hist-Model and W-RCP8.5, respectively, and in the eastern Caribbean with ~ -1 cm/decade for W-RCP8.5 (Fig. 7). They are however modest compared with year-to-year variations and inter-member spread: standard deviation and confidence interval width range from 3 to 10 cm and from 6 to 12 cm, respectively. These results exhibit little sensitivity to horizontal resolution of wind and waves, at least in the MDR and eastern Caribbean that are included in the MFWAM01 domain (Fig. 8a, b). This is because projected changes in seasonal means mostly result from changes in large-scale atmospheric patterns as argued here.

3.2.2 TC-related wave climate

The spatial pattern of W-Hist-Model TC-related H_s (i.e. the hurricane-season mean contribution of TCs to H_s , contours on Fig. 9a) is qualitatively similar to the Hist-Model frequency of TC days (contours on Fig. 1), suggesting that the methodology described in 2.2.2 is adequate. Indeed, TC-related wave heights are highest around Bermuda near $30\text{--}35^\circ\text{N}$, 65°W (~ 0.45 m i.e. $\sim 25\%$ of mean H_s) and extend from the tropics to the mid-latitudes, particularly in the sub-basin western half. Compared to TC activity (Fig. 1), the H_s pattern is somewhat smoother and more isotropic (Fig. 9a). This is mostly because of swell propagation away from TC-induced wind fetches. The corresponding H_{s0} pattern is more zonal and closer to TC-day frequency (Fig. 9b, contours) compared to the wider and smoother H_{s1} pattern (Fig. S4a, contours): meridional scales are ~ 3500 km and ~ 2000 km



for H_{s1} and H_{s0} , respectively, as inferred from the 0.05 m contour.

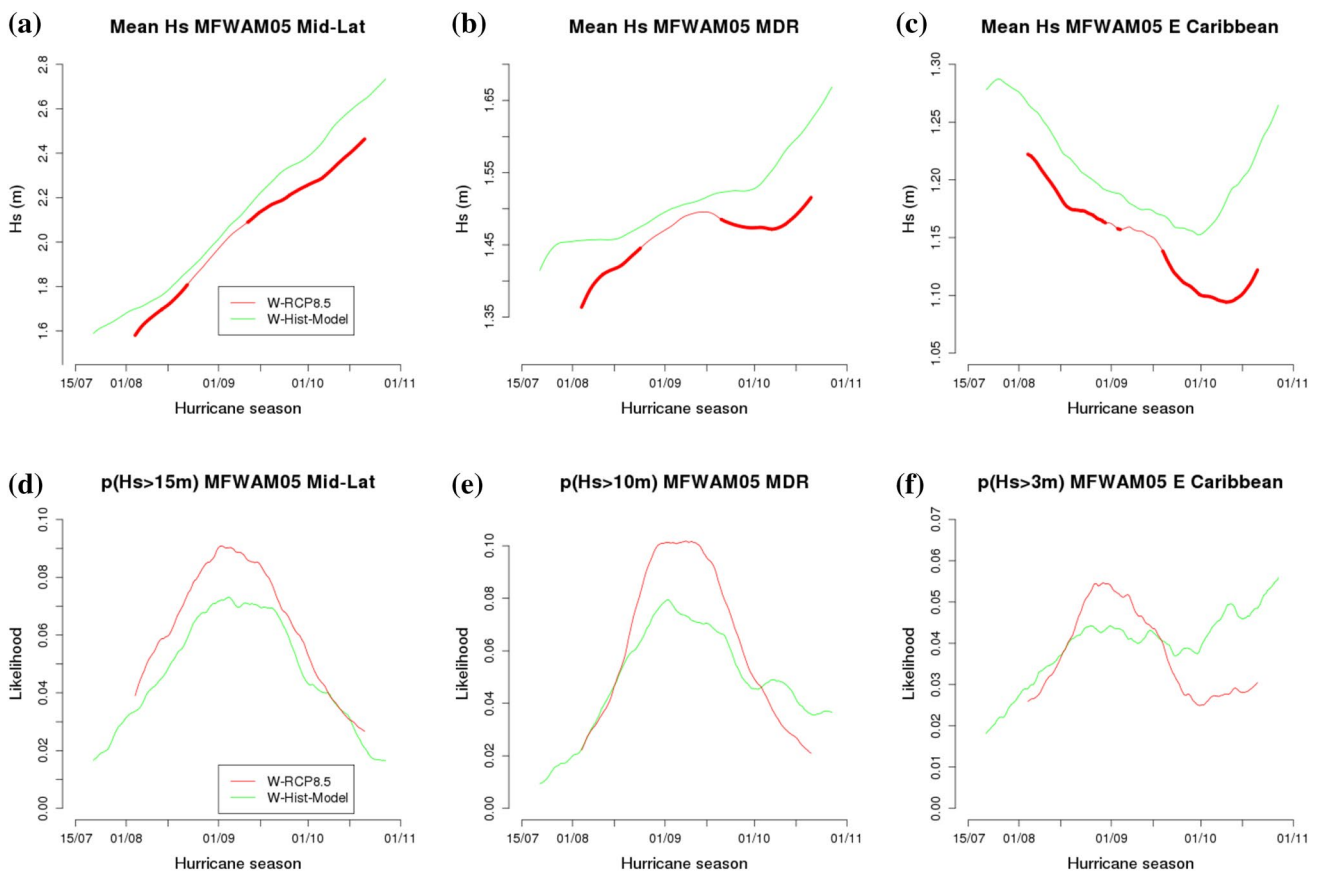


Fig. 6 **a–c** Mean significant wave height H_s (m) for each calendar 3-h time step during the hurricane season from MFWAM05 W-RCP8.5 (2051–2080, red) and W-Hist-Model (1984–2013, green) simulations over the **a** mid-latitudes (30–50°N, 20–80°W), **b** MDR (5–28°N, 10–75°W), and **c** eastern Caribbean (11.7–19°N, 59–64°W). **d–f** Ensemble mean likelihood (over 30 years) that the maximum significant wave height H_s over **d** the mid-latitudes exceeds 15 m, **e** the

MDR exceeds 10 m, and **f** the eastern Caribbean exceeds 3 m for each calendar 3-h time step during the hurricane season from MFWAM05 W-RCP8.5 (red) and W-Hist-Model (green) simulations. Thick red lines are for differences W-RCP8.5 minus W-Hist-Model significant at the 5% level (Online Resource 1, Sects. 2 and 4). A 30-day moving average was applied to filter out high-frequency noise

The pattern of projected future changes in TC-related H_s (shading on Fig. 9a) is also somewhat similar to changes in TC activity (shading on Fig. 1), with widespread 2–5 cm reduction across the sub-basin and 3–4 cm increases off the African continent and northeastern United States. However, notable differences are found. The increase off Cape Verde extends all the way across the MDR into the Caribbean Sea, while that off New England does not extend across the sub-basin mid-latitudes, unlike the increase in TC activity (Fig. 1). Even more importantly, the projected changes in TC-related H_s are not statistically significant. This is also the case for H_{s1} (Fig. S4a) and T_m (Fig. S4b), but not for H_{s0} , which exhibits a significant 2–5 cm increase across most of the MDR (Fig. 9b). Although a closer relationship with wind changes is expected for H_{s0} compared to other variables, this finding is somewhat surprising, as these changes extend much farther west compared to those in TC frequency (Fig. 1).

Projected changes in TC activity only considered the locations of TC centers (Chauvin et al. 2020) and not the large associated wind fetches considered in H_{s0} , which may be one explanation. Alternatively, TCs around Cape Verde may be associated with background conditions that favor enhanced U_{10} in the trade wind belt.

Conversely to mean wave heights, expected changes in TC-related wave heights show some sensitivity to spatial resolution of winds and waves. Indeed, while the magnitude of projected changes in MDR TC-related H_{s0} is similar in MFWAM01 (Fig. 9d) and MFWAM05 (Fig. 9b), the former are significant over wider regions. In particular, the increase in MFWAM01 TC-related H_{s0} is significant not only west of Cape Verde but also east of the archipelago all the way up to the African continent. This may be related to small-scale wind changes in the region of sharp increase in TC activity (Fig. 1) being better accounted for in the higher-resolution wave model. On the other hand, projected changes

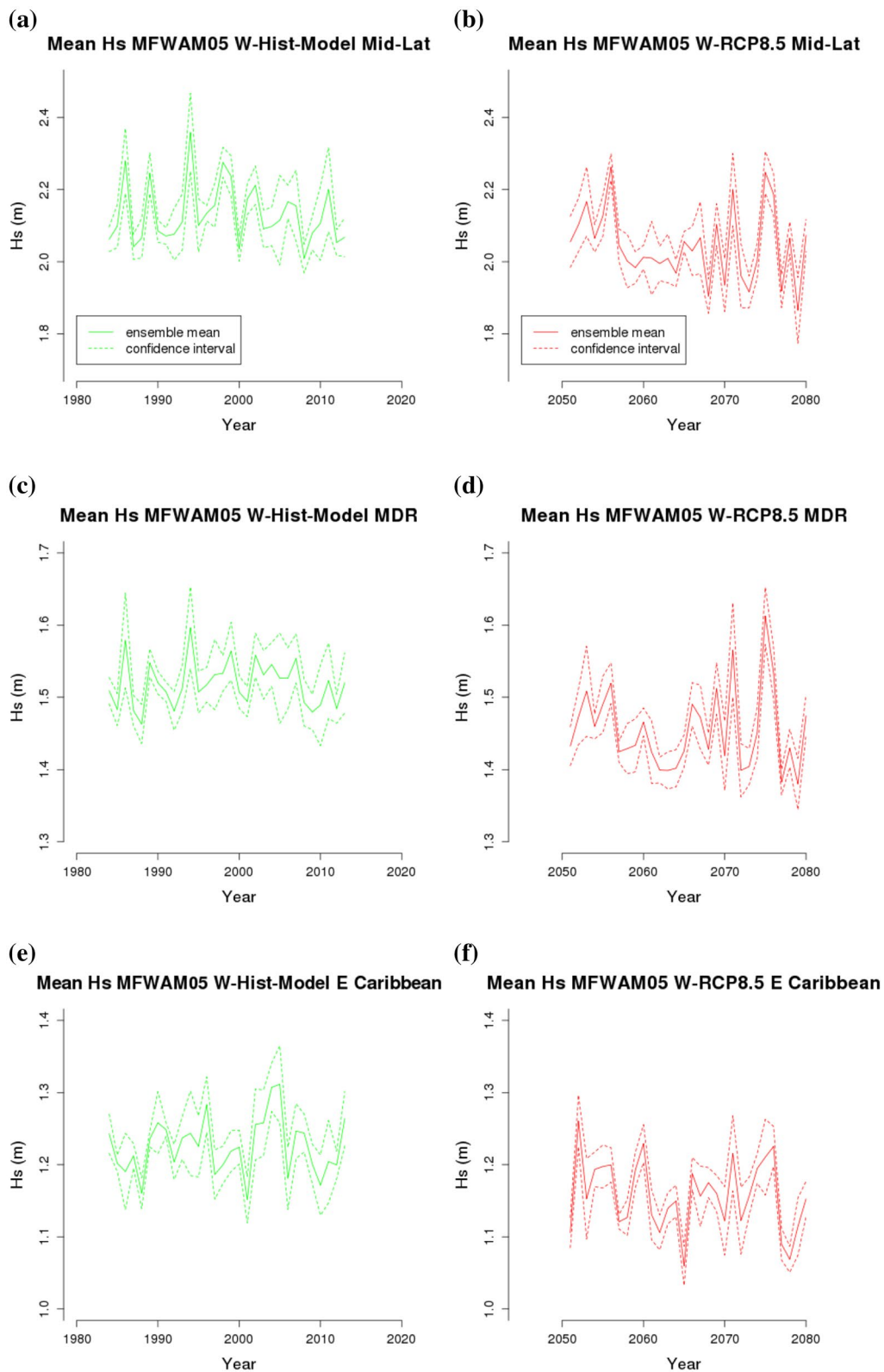


Fig. 7 Annual time series of hurricane-season mean significant wave height H_s (m) from MFWAM05 (a, c, e) W-Hist-Model (1984–2013, solid green line) and (b, d, f) W-RCP8.5 simulations (2051–2080,

solid red line) over the (a, b) mid-latitudes, (c, d) MDR, and (e, f) eastern Caribbean. The dashed green/red lines indicate the associated confidence intervals (Online Resource 1, Sect. 5)

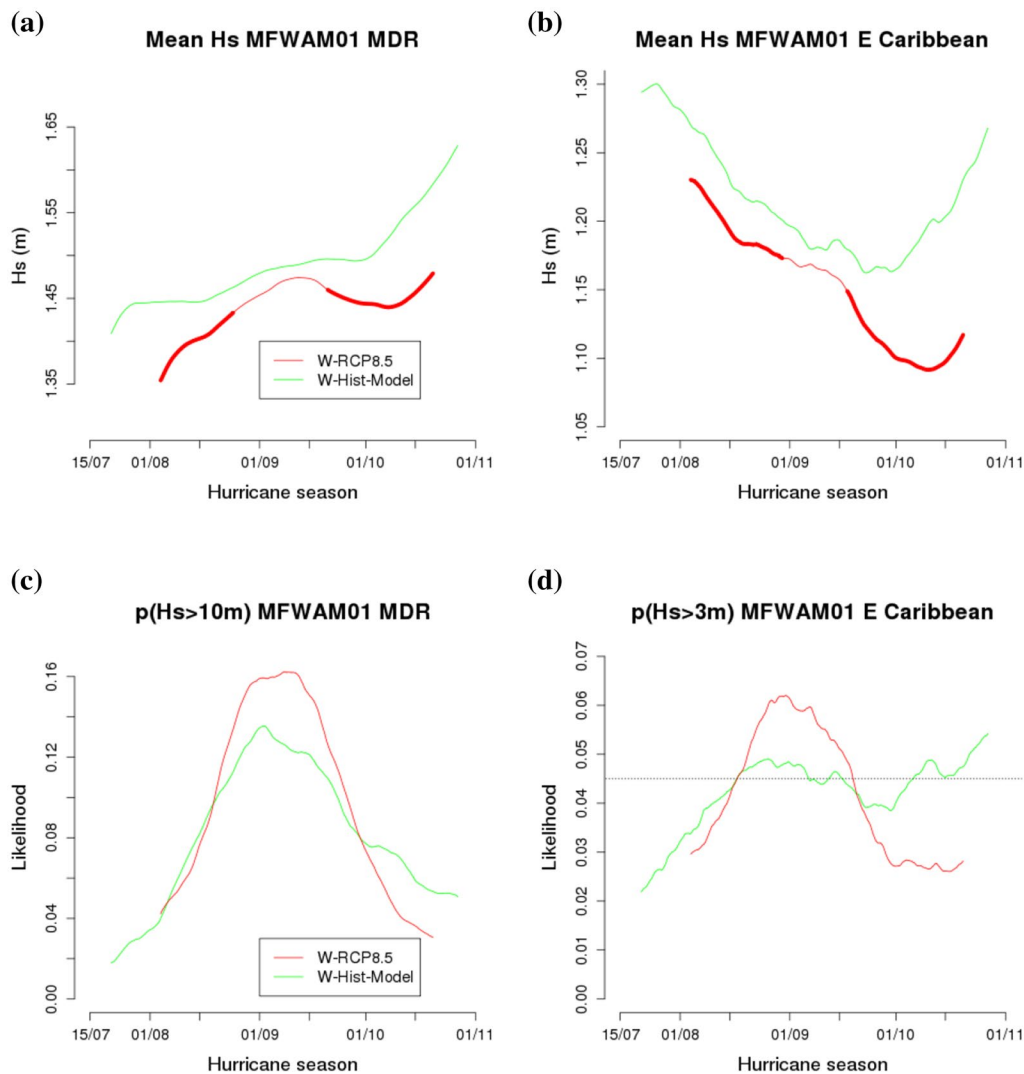


Fig. 8 **a, b** Same as Fig. 6b, c and **(c, d)** same as Fig. 6e, f, except from MFWAM01. The horizontal dotted line on **d** indicates the threshold used to define the hurricane season peak phase (4.5% i.e. 1.35 years)

in TC-related H_s , H_{s1} , and T_m are not very sensitive to resolution (Fig. 9a, c, S4).

3.2.3 Extreme TC-related wave heights

In W-Hist-Model, 10-year TC-related H_s during the hurricane season range from 2–3 m in the equatorial Atlantic to 15–16 m near 60°W, 40°N off northeastern United States (contours on Fig. 10a). Such a pattern is broadly consistent with mean TC-related H_s (Fig. 9a) but slightly displaced northeastward. Unlike mean TC-related H_s , it also presents a broad, homogeneous pattern of elevated values (10–11 m) north of 50°N. This is likely a residual signal mostly from non-TC-related H_s : 10-year H_s computed over both TC and non-TC days exhibits a secondary maximum near 60°N (not shown). ‘Post-TCs’ resulting

from extratropical transitions may also play a role, particularly because of lagged wave response to winds due to wave growth in developing seas and swell propagation after TC decay (see Sect. 4.5).

Nevertheless, restricting the computation of 10-year TC-related H_s to the season peak yields a sharper decay north of ~45°N while conserving a maximum at 40°N with values ~14 m (contours on Fig. 10b). Indeed, the analysis of MFWAM01 extreme wave heights leads to the definition of the following periods for the season peak (see Sect. 2.2.1): August 17 to September 15 for W-Hist-Model and August 17 to September 18 for W-RCP8.5 (Fig. 8d). These findings are consistent with stronger TC activity and weaker mid-latitude storm activity from mid-August to mid-September compared to late hurricane season in October–November. Note that 10-year TC-related H_s are slightly larger when computed

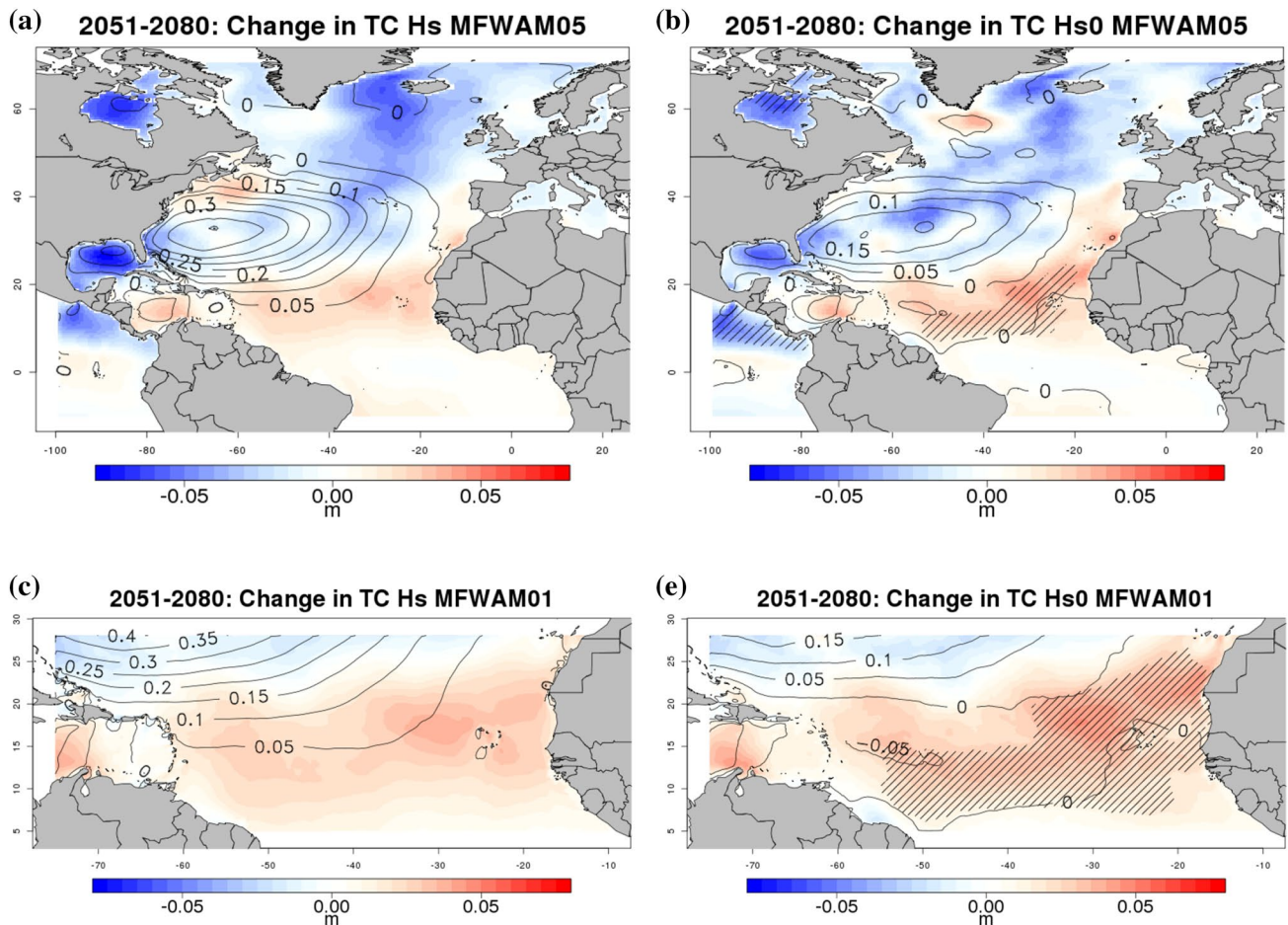


Fig. 9 Projected changes in mean TC-related (**a, c**) significant wave height H_s (m) and (**b, d**) significant height of wind waves H_{s0} (m) from (**a, b**) MFWAM05 and (**c, d**) MFWAM01 between W-RCP8.5

(2051–2080) and W-Hist-Model (1984–2013). W-Hist-Model values for H_s and H_{s0} are overlaid as black contours. Hatchings are for the 5% significance level

over the entire season (Fig. 10a, b) because annual maxima occasionally occur outside of the season peak.

Repeating the analysis for H_{s1} and H_{s0} yields similar patterns (contours on Fig. S5). The gradient of extreme wave heights between the northwestern part of the basin and the MDR is however larger for H_{s0} compared to H_{s1} : maximum values near 40°N exceed 12/15 m (respectively 8/10 m) for H_{s0} (respectively H_{s1}) over the season peak/whole season, and decrease below 2 m (respectively 3 m) near $5\text{--}10^\circ\text{N}$. Smoother variations in H_{s1} are consistent with hurricane swell propagation over large distances. Interestingly, a secondary maximum near 60°N in 10-year TC-related H_{s0} only arises when the analysis extends over the whole season (Fig. S5c) and is not seen for H_{s1} (Fig. S5ab). It is again consistent with extratropical storm rather than TC forcing north of 45°N .

Under RCP8.5 climate, 10-year TC-related H_s , H_{s1} , and H_{s0} increase markedly over the hurricane season near the central and northern US East Coast by up to 2–3 m (shading

on Fig. 10a, S5ac), although only limited areas southeast of Cape Hatteras, Cape Cod, and Nova Scotia experience statistically significant changes. Chauvin et al. (2020) found a statistically significant increase in the intensity of major hurricanes over the North Atlantic. However, this result may not apply locally where the largest expected changes in extreme wave heights are found. Indeed, since TC tracks are also projected to change (Chauvin et al. 2020), finding localized robust changes is not straightforward. Instead, projected changes in the spatial structure, lifetime, phase speed or trajectories of major hurricanes might favor more efficient growth as waves propagate away from the storm center, consistently with the wider patch of significant H_{s1} increase (Fig. S5a).

A 1–2 m increase in 10-year TC-related H_s is also found within the MDR along a northwest-southeast oriented band extending from Cape Verde to $\sim 60^\circ\text{W}$, 20°N , but is only significant near 30°W (Fig. 10a). Unlike the increase in the northwestern Atlantic, it is associated with a statistically

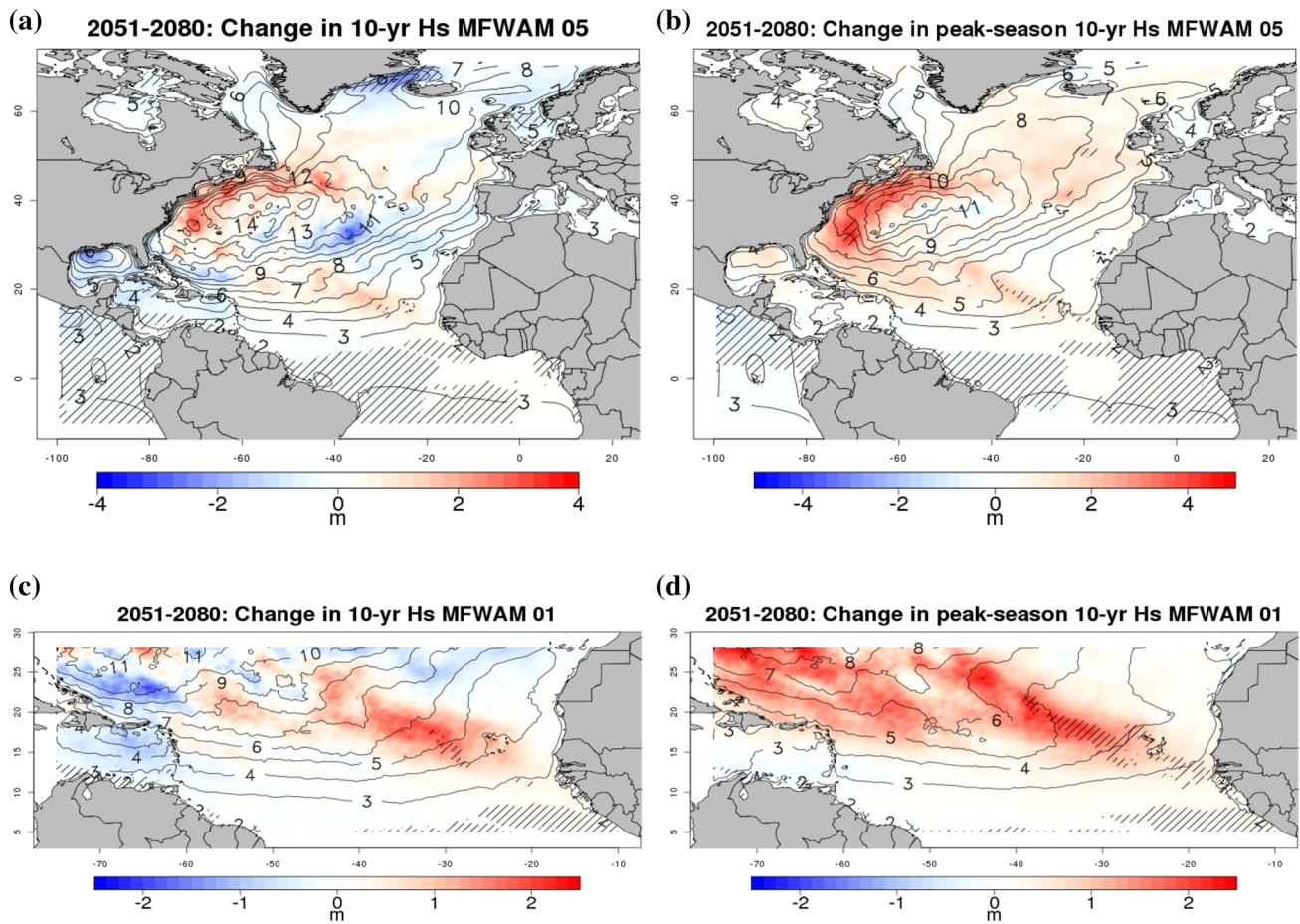


Fig. 10 Projected changes in 10-year TC-related significant wave height H_s (m) from (a, b) MFWAM05 and (c, d) MFWAM01 during (a, c) the hurricane season and (b, d) its peak phase between

W-RCP8.5 (2051–2080) and W-Hist-Model (1984–2013). W-Hist-Model values are overlaid as black contours. Hatchings are for the 5% significance level

significant increase in H_{s0} rather than H_{s1} (Fig. S5ac). This is consistent with the strong increase in TC activity around Cape Verde reported by Chauvin et al. (2020) and the significant increase in TC-related H_{s0} in the MDR (Fig. 9b, d). Further south and closer to the equator, a robust reduction in extreme H_s , H_{s1} , and H_{s0} is also found. Its extension and orientation are similar to those of the extreme wave height increase, suggesting both may combine to form a dipole, possibly associated with poleward displacement of extreme wave heights. In fact, projected TC frequency changes exhibit a similar dipole (Fig. 1).

When the projected changes in extreme wave heights are restricted to the season peak (Fig. 10b, S5bd), they are larger (over 4-m H_s increase off the US East Coast), mostly positive, and more robust in the MDR and northwestern Atlantic. This again is consistent with Chauvin et al. (2020) who found an overall reduction in TC numbers over the season (see the widespread decrease on Fig. 1), yet a strong increase in September with a pattern similar to those found for extreme wave heights (Chauvin et al. 2020, their Fig. 10).

The comparison of projected changes in MDR 10-year wave heights between MFWAM05 and MFWAM01 illustrates the sensitivity of our results to resolution (see also Sect. 3.2.2). The magnitude of these changes is similar in the two grids (Fig. 10) but they are statistically significant over slightly wider areas in MFWAM01. These results are qualitatively consistent with those found for MDR TC-related H_{s0} (Fig. 9b, d) and advocate for increased model resolution including wave models, not just the GCMs.

Projected changes in the return periods of extreme wave heights depending on the season phase (early season, peak phase, late season) are also of interest. The likelihood that wave heights exceed certain thresholds within the mid-latitudes, MDR, and eastern Caribbean varies through the season (Fig. 6d–f), as anticipated from seasonal variations in TC activity (Fig. 2). For both W-Hist-Model and W-RCP8.5, the frequency of extreme wave heights increases sharply after late July/early August, reaches a maximum a month later, before decaying again in the second half of October. In the eastern Caribbean, extreme wave height frequency

rises again in early October (Fig. 6f), which may result from remote swells of extratropical origin rather than TC-related storm waves.

Future projections show changes similar to those in TC numbers (maximum number of TC years rises by 7% from ~16.2 for Hist-Model to ~17.4 for RCP8.5, Fig. 2): a 20–30% increase in August–September in the three regions, although not statistically significant (Fig. 6d–f). The sign of the change in the early and late seasons is however region-dependent: an increase in the mid-latitudes (Fig. 6d), little change in the MDR (Fig. 6e), and a decrease in the eastern Caribbean (Fig. 6f). Although none of these regions exhibits statistically significant increases in extreme wave event frequency during the season peak (Fig. 6d–f), the lack of significance for the concurrent decrease in mean wave heights (Fig. 6a–c) suggests that the increase may be robust. In the tropical North Atlantic, the frequency of wave extremes decreases in October, possibly because of concurrent reductions in the frequency of mid-latitude storms and associated swells. On the other hand, strong interannual variations and inter-member spread in W-Hist-Model and W-RCP8.5 complicate the detection of long-term trends in wave extremes to an even greater extent than mean H_s (Fig. 11): standard deviations are typically ~0.02 i.e. 45–90% of the mean, and confidence interval width is ~0.03 on average.

Similarly to mean TC-related H_{s0} and 10-year TC-related H_s (Figs. 9b, d, 10), the frequency of extreme wave heights is sensitive to the spatial resolution of winds and waves (Fig. 8c, d, S6), particularly within the MDR: extreme H_s values are much more frequent with increased resolution, consistently with Timmermans et al. (2017) and Chen et al. (2018). The associated projected future changes are however still not statistically significant.

4 Discussion

4.1 Choice of GCM, prescribed SST, and GHG forcing

An obvious limitation to this study is the use of a single combination of GCM, prescribed SST, and GHG emission scenario. Considering more combinations would help better quantify uncertainties, but is beyond the scope of this study because of constraints set by computational cost and lack of resources. Nevertheless, our projections of TC activity are consistent with previous studies. Key results include reduced TC numbers, increased proportion and intensity of major hurricanes, poleward displacement of TC activity to some extent (Chauvin et al. 2020, Fig. 1), and slightly shorter hurricane season (Fig. 2; Table 3, see also Diro et al. 2014). Therefore and despite the uncertainties, our results represent an ocean wave response to projections of TC activity that are consistent with state-of-the-art knowledge.

4.2 Wave model calibration and bias correction

The use of a single wave model is another important source of uncertainty, which may be reduced with further calibration and improved physics (Morim et al. 2019). In particular, only a partial sensitivity study of H_s bias to the wave growth coefficient β_{max} was conducted and led to the use of a value of 1.13 that is substantially lower than in the operation configuration (1.52, lowered in 2018 to 1.48). An intermediate value of 1.30 was tested, but more exhaustive study may have led to slightly larger or lower value than 1.13.

Lemos et al. (2020) underlined the importance of bias correction that is widely used in climate impact studies (e.g. Déqué 2007; Cantet et al. 2014) but hardly for wave climate projections (Charles et al. 2012). Using the GOW2 hindcast that reproduces extreme TC wave heights remarkably well (Perez et al. 2017), they show that mean and extreme present-climate H_s can be efficiently corrected, and that future projections are sensitive to such corrections. The authors however considered coarse-resolution GCMs (1–3°) and wave models (1°) that cannot grasp the magnitude and small-scale structure of TC winds and waves, unlike our high-resolution models. Therefore, correcting our simulations may not improve TC wave heights as significantly as Lemos et al. (2020) did. Nevertheless, future research should consider calibration and bias correction for further control of model bias and reduced uncertainties.

4.3 Lack of ocean/atmosphere/wave coupling

Projected changes in extreme H_s are related to those found for major hurricanes by Chauvin et al. (2020). Although ARPEGE-Climat reproduces the distribution of Atlantic TC intensities fairly well, the authors recognize a tendency for overestimation. They argue that it may result from a lack of small-scale air-sea coupling, among other factors such as details of the turbulence scheme (Roberts et al. 2020a). Indeed, uncoupled simulations lack the wind-driven ocean cooling through vertical mixing and upwelling and consequent feedback to the atmosphere (e.g. Jullien et al. 2014). The very large changes in extreme H_s expected over parts of the North Atlantic may thus be overestimated. Future work should consider high-resolution coupled GCM forcing, which is starting to become available as high-performance computing continues to progress rapidly (Roberts et al. 2020b).

Wave-atmosphere coupling is also important for TCs. Chen and Yu (2017) showed that wave simulations driven by Hurricane Katrina (2005) are significantly improved when a wave boundary layer model (WBLM, Moon et al. 2004) is used to compute wind stress, compared to standard bulk formula. MFWAM includes a wind stress parameterization that accounts for wave effects on sea surface roughness and

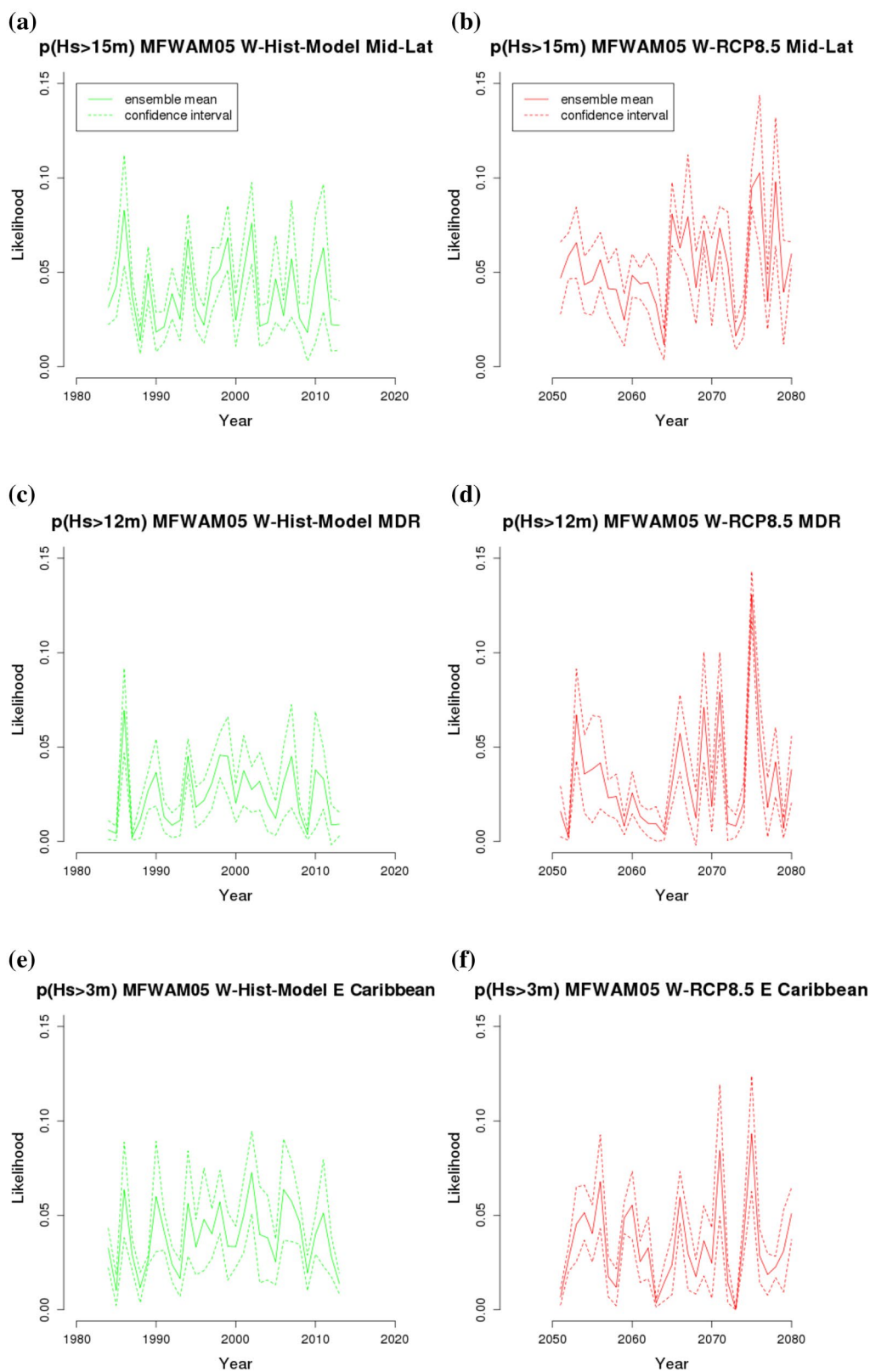


Fig. 11 Annual time series of the likelihood (over the hurricane season) that the maximum significant wave height H_s from MFWAM05 (a, c, e) W-Hist-Model (1984–2013, solid green line) and (b, d, f) W-RCP8.5 simulations (2051–2080, solid red line) over (a, b) the

mid-latitudes exceeds 15 m, (c, d) the MDR exceeds 12 m, and (e, f) the eastern Caribbean exceeds 3 m. The dashed green/red lines indicate the associated confidence intervals (Online Resource 1, Sect. 5)

effectively reduces the drag coefficient for high winds (Ardhuin et al. 2010), as expected from TC wind observations (Powell et al. 2003). Its efficiency compared to other parameterizations (e.g. WBLM) has however not been assessed and may be improved. For example, introducing a cut-off frequency for the wave spectrum further limits the drag coefficient for strong winds in a newer version of MFWAM (Aouf et al. 2018).

Improvements in TC wave projections will continue gradually, incorporating one feedback loop at a time before a fully coupled ocean–atmosphere–wave model may be built.

4.4 Child model nesting

Our choice for the nested model domain is retrospectively questionable. First, because Chauvin et al. (2020) found that MDR TC numbers are underestimated by a factor two. And second, because the largest increases in extreme H_s were found elsewhere, in the northwestern Atlantic. Future studies shall improve the spatial distribution of TC activity, and downscale wave models right where projected changes in extreme H_s are strongest. Besides, high-resolution runs with either high- or coarse-resolution winds could be used to disentangle the roles of TC wind distributions and small-scale wave processes.

4.5 Selection of TC days

The chronological approach based on TC days and used to eliminate non-TC related sea states has limitations. For instance, extratropical storms sometimes occur simultaneously with TCs further south, and their effects are erroneously included. Yet, such artefacts are likely modest given the focus on the hurricane season (mid-latitude storms are more active in winter) and the generally uncorrelated tropical and extratropical drivers. An additional complexity is however introduced by the extratropical transition that TCs often undergo during their decaying phase (Bieli et al. 2019a, b). This is particularly true for Chauvin et al. (2020)'s ARPEGE-Climat simulations that overestimate subtropical North Atlantic TC activity.

Most previous studies have similar limitations. Fan et al. (2013) and Timmermans et al. (2017) presented projections of extreme wave heights and compared them qualitatively with projected TC activity, without explicit criteria to extract TC wave signals. Appendini et al. (2017) used a methodology similar to ours by computing extremes over each TC event. Their domain was however limited to the Gulf of Mexico, thus focusing on wind sea by construction and avoiding the issue of the attribution to other drivers.

An exception is the study of western North Pacific TC wave projections by Shimura et al. (2015), where TC waves are determined from TC center locations considering a

500-km radius. TC tracks were obtained by Murakami et al. (2012) with a methodology similar to ours. Such geolocalization has not been considered here because hurricane swell can propagate over much larger distances (Zelinsky 2019). The benefit of our approach is that extreme wave heights outside TC regions but subject to such remote swells are accounted for. In addition to a residual effect from non-TC-related extremes, the lack of georeferencing may however lead to underestimated TC wave climate and future projection outside TC regions, as suggested by the not statistically significant changes in TC-related H_s and H_{s1} (Fig. 9a, c, S4ac).

A limitation to both this study and Shimura et al. (2015) is that no delay was considered between TC tracks and associated sea states. Therefore, the propagation of swell generated during TC decaying phase is mostly not accounted for. The solution is not straightforward. Such delay should depend on storm intensity, structure and translation velocity, which affect wind fetches, wave periods and ultimately, swell phase speeds. It was however not considered critical for wave extremes because at most locations over long periods, these should be driven by TC lifetime maximum winds before the decaying phase (except maybe for mid-latitude H_{s0} , Fig. S5c).

4.6 Definition of the hurricane season

The method based on the seasonality of TC return periods (see Sect. 2.2.1) relies on objective criteria and may provide a benchmark for GCMs to reproduce the season dates compared to best-track data. It however depends on the somewhat arbitrary choice of a return period threshold. Nevertheless, TC return periods in the historical runs agree well with IBTrACS even in June and November (Fig. 2), meaning that if it were not for computational constraints, a lower threshold (e.g. a 10-year return period) could have been used to more closely match the WMO standard. On the other hand, the projected season shortening would have been more pronounced in such case (Fig. 2), suggesting potential sensitivity of our results to this choice. In addition, the application to other numerical models may yield different dates, complicating any comparison between different studies. As such, it raises the question of reproducibility, which is particularly important for climate projection studies as emphasized by coordinated community efforts such as CMIP or COWCLIP.

Fixed, standard dates have the advantage of simplicity and easier reproduction, despite undesired effects in case of shifting future seasons. ASO is the longest sequence of complete months within the W-Hist-Obs, W-Hist-Model and W-RCP8.5 hurricane seasons (Table 3). It lies at the core of the observed season (Fig. 2), therefore providing a relevant testbed for future studies. The sensitivity of some of our key results to the alternative choice of the ASO period was

then assessed for this purpose. It was found to be weak, as illustrated by the comparison of Figs. S7, S8 with Figs. 5, 10a, S5ac, suggesting that the conclusions drawn here are not much sensitive to the choice of the exact time period used to represent the hurricane season. The same holds for the season peak. Indeed, the peak of TC activity, around mid-August to mid-September in the model and IBTrACS (Fig. 2), tends to be in phase with the peak of extreme wave activity not only in the eastern Caribbean but also in the mid-latitudes and MDR (Figs. 6d–f, 8c, d).

4.7 Statistical significance

The robustness of wave climate projections in this paper is assessed with various approaches used to compute statistical significance at the standard 5% level (Online Resource 1, Sects. 1–4). According to these, some projected changes were very robust, namely those in mean U_{10} and H_s that appear statistically significant over the whole sub-basin (Fig. 5a, b) and most of the hurricane season (Fig. 6a–c). Others are significant at specific locations only, e.g. changes in TC numbers, TC-related H_{s0} , or 10-year return levels (Figs. 1, 9b, d, 10). Finally, a few changes were not found significant at all, such as exceedance probabilities for extreme H_s thresholds or TC-related H_s (Figs. 6d–f, 9a, c).

The reader is however advised against systematically dismissing results that are not statistically significant (and taking significant results for granted) because this is not unambiguous evidence of the null hypothesis, as emphasized by Amrhein et al. (2019). The $p < 0.05$ threshold is not only arbitrary, it can erroneously lead to opposed conclusions from studies using very similar data. Additional evidence including physical arguments needs to be considered before drawing conclusions. For example, we relate the non-significant yet sharp peak-season increase in extreme H_s to the concurrent mean H_s decrease, which is smallest and not significant only then (Fig. 6). Although not statistically significant, the increases in MDR TC-related H_s and H_{s1} are consistent with significant increases in H_{s0} and in Cape Verde TC numbers (Figs. 1, 9, S4). This may be particularly relevant for 10-year H_s , for which a conservative and somewhat subjective method had to be adopted (Online Resource 1, Sect. 4). The associated changes may be robust over wider areas than those hatched on Fig. 10 (see also Figs. S5, S8), as suggested by widespread and strong increases in TC regions particularly at the season peak ($\sim +2$ to $+5$ m), and by the similar pattern of projected September increases in TC numbers (Chauvin et al. 2020).

4.8 Implications for future work

While TCs make a major contribution to the climatology of extreme wave events in the North Atlantic, mid-latitude

storm activity is also a recurrent seasonal source of energy for large wind sea during winter, roughly from November to April. The associated powerful remote swells affect shorelines across the sub-basin and as far south as the eastern Caribbean, thousands of kilometers away where they can cause significant damage (Jury 2018). The smaller islands of the Lesser Antilles are particularly vulnerable to large ocean wave events of both TC and extratropical origin and to the associated storm surge hazard because of their isolation, limited surface and densely populated shorelines, among other factors. Incoming ocean swells are modified by a range of complex processes occurring at both the island and regional scales due to the north–south alignment of islands located in the path of these swells. How future projections of TC-related and mid-latitude extreme wave climate will affect shorelines of small tropical islands such as the Lesser Antilles is a key question from both societal and scientific points of view. The modeling framework presented in this study may then serve as an appropriate framework for downscaled projections over the Lesser Antilles at sub-kilometer-scale resolution in order to address this question. This will be the topic of future research.

5 Conclusion

High-resolution ensemble atmospheric GCM simulations under present and future RCP8.5 climates were used to drive basin-scale 50-km wave simulations for the Atlantic Ocean and nested 10-km simulations for the TC main development region (MDR) to infer projected future changes in North Atlantic TC-related wave climate. Overall realistic GCM mean low-level circulation and TC characteristics allowed obtaining plausible projections in the associated wave response.

Our main conclusions include a large-scale decrease in average wave heights throughout the hurricane season driven by a weaker and poleward-displaced anticyclone, yet concurrent increases in extreme TC-related wave heights in the MDR associated with stronger TC activity around Cape Verde and related changes in wind sea. The largest expected changes in extreme wave heights were however found near the coast of northeastern United States, possibly related to slight poleward displacement of TC activity, and highest during the season peak phase from mid-August to mid-September. Changes were found to be statistically robust in some specific areas.

Supplementary Information The online version contains supplementary material available at <https://doi.org/10.1007/s00382-021-05664-5>.

Acknowledgements We are grateful to two anonymous reviewers whose detailed and constructive comments greatly helped improve

the quality of the original manuscript. We acknowledge L. Aouf for advice with MFWAM calibration/validation, D. Paradis, P. Cantet and R. Osinski for fruitful discussions, and P.-C. Dutrieux for help with post-processing algorithms. The altimeter wave data were obtained from the ESA CCI Sea State project. This effort is sponsored by the European Regional Development Fund, Guadeloupe region, grant CR/16-115 C3AF (Changement Climatique et Conséquences sur les Antilles Françaises).

References

- Alves JHGM (2006) Numerical modeling of ocean swell contributions to the global wind-wave climate. *Ocean Model* 11:98–122
- Amrhein V et al (2019) Retire statistical significance. *Nature* 567:305–307. <https://doi.org/10.1038/d41586-019-00857-9>
- Aouf L (2018) CMEMS quality information document for global ocean waves analysis and forecasting product. CMEMS-GLO-QUID-001_027 <http://resources.marine.copernicus.eu/documents/QUID/CMEMS-GLO-QUID-001-027.pdf>. Accessed 8 Oct 2019
- Appendini CM, Pedrozo-Acuña A, Meza-Padilla R, Torres-Freyermuth A, Cerezo-Mota R, Lopez-Gonzalez J, Ruiz-Salcines P (2017) On the role of climate change on wind waves generated by tropical cyclones in the Gulf of Mexico. *Coast Eng J* 59:2. <https://doi.org/10.1142/S0578563417400010>
- Ardhuin F, Rogers E, Babanin AV, Filipot JF, Magne R, Roland A, van der Westhuysen A, Queffelec JM, Lefevre JM, Aouf L, Collard F (2010) Semiempirical dissipation source functions for ocean waves. Part I: definition, calibration, and validation. *J Phys Oceanogr* 40(9):1917–1941
- Batté L, Déqué M (2016) Randomly correcting model errors in the ARPEGE-Climate v6.1 component of CNRM-CM: applications for seasonal forecasts. *Geosci Model Dev* 9:2055–2076. <https://doi.org/10.5194/gmd-9-2055-2016>
- Bieli M, Camargo SJ, Sobel AH, Evans JL, Hall T (2019a) A global climatology of extratropical transition. Part I: characteristics across basins. *J Clim* 32:3557–3582. <https://doi.org/10.1175/JCLI-D-17-0518.1>
- Bieli M, Camargo SJ, Sobel AH, Evans JL, Hall T (2019b) A global climatology of extratropical transition. Part II: statistical performance of the cyclone phase space. *J Clim* 32:3583–3597. <https://doi.org/10.1175/JCLI-D-18-0052.1>
- Camus P, Losada IJ, Izaguirre C, Espejo A, Menéndez M, Pérez J (2017) Statistical wave climate projections for coastal impact assessments. *Earth's Fut* 5:918–933. <https://doi.org/10.1002/2017EF000609>
- Cantet P, Déqué M, Palany P, Maridet JL (2014) The importance of using a high-resolution model to study the climate change on small islands: the lesser antilles case. *Tellus A* 66:24065. <https://doi.org/10.3402/tellusa.v66.24065>
- Cantet P, Belmadani A, Chauvin F, Palany P (2020) Projections of tropical cyclone rainfall over land with an Eulerian approach: case study of three islands in the West Indies. *Int J Climatol* 1–11. <https://doi.org/10.1002/joc.6760>
- Charles E, Idier D, Delecluse P, Déqué M, Le Cozannet G (2012) Climate change impact on waves in the Bay of Biscay, France. *Ocean Dyn* 62:831–848. <https://doi.org/10.1007/s10236-012-0534-8>
- Chauvin F, Royer JF, Déqué D (2006) Response of hurricane-type vortices to global warming as simulated by ARPEGE-Climat at high resolution. *Clim Dyn* 27:377–399
- Chauvin F, Pilon R, Palany P, Belmadani A (2020) Future changes in Atlantic hurricanes with the rotated-stretched ARPEGE-Climat at very high resolution. *Clim Dyn* 54:947–972. <https://doi.org/10.1007/s00382-019-05040-4>
- Chen Y, Yu X (2017) Sensitivity of storm wave modeling to wind stress evaluation methods. *J Adv Model Earth Sys* 9:893–907. <https://doi.org/10.1002/2016MS000850>
- Chen X, Ginis I, Hara T (2018) Sensitivity of offshore tropical cyclone wave simulations to spatial resolution in wave models. *J Mar Sci Eng* 6:116. <https://doi.org/10.3390/jmse6040116>
- Christensen JH, Krishna Kumar K, Aldrian E, An SI, Cavalcanti IFA, de Castro M, Dong W, Goswami P, Hall A, Kanyanga JK, Kitoh A, Kossin J, Lau NC, Renwick J, Stephenson DB, Xie SP, Zhou T (2013) Climate phenomena and their relevance for future regional climate change. In: Stocker, TF, Qin D, Plattner GK, Tignor M, Allen SK, Boschung J, Nauels A, Xia Y, Bex V, Midgley PM (eds) *Climate change 2013: the physical science basis. Contribution of working group I to the fifth assessment report of the intergovernmental panel on climate change*. Cambridge University Press, Cambridge, United Kingdom and New York, NY, USA
- Church JA, Clark PU, Cazenave A, Gregory JM, Jevrejeva S, Levermann A, Merrifield MA, Milne GA, Nerem RS, Nunn PD, Payne AJ, Pfeffer WT, Stammer D, Unnikrishnan AS (2013) Sea level change. In: Stocker, TF, Qin D, Plattner GK, Tignor M, Allen SK, Boschung J, Nauels A, Xia Y, Bex V, Midgley PM (eds) *Climate change 2013: the physical science basis. Contribution of working group I to the fifth assessment report of the intergovernmental panel on climate change*. Cambridge University Press, Cambridge, United Kingdom and New York, NY, USA
- Dee DP et al (2011) The ERA-Interim reanalysis: configuration and performance of the data assimilation system. *Q J R Meteorol Soc* A 137:553–597. <https://doi.org/10.1002/qj.828>
- Déqué M (2007) Frequency of precipitation and temperature extremes over France in an anthropogenic scenario: model results and statistical correction according to observed values. *Glob Planet Chang* 57:16–26
- Diro GT, Giorgi F, Fuentes-Franco R, Walsh KJE, Giuliani G, Coppola E (2014) Tropical cyclones in a regional climate change projection with RegCM4 over the CORDEX Central America domain. *Clim Change* 125:79–94. <https://doi.org/10.1007/s10584-014-1155-7>
- Dodet G et al (2020) The Sea State CCI dataset v1: towards a sea state climate data record based on satellite observations. *Earth Sys Sci Data* 12:1929–1951. <https://doi.org/10.5194/essd-12-1929-2020>
- Emanuel KA (2013) Downscaling CMIP5 climate models shows increased tropical cyclone activity over the 21st century. *Proc Natl Acad Sci USA* 110:12219–12224. <https://doi.org/10.1073/pnas.1301293110>
- Fan Y, Held IM, Lin SJ, Wang XL (2013) Ocean warming effect on surface gravity wave climate change for the end of the twenty-first century. *J Clim* 26:6046–6066
- Fan Y, Lin SJ, Griffies SM, Hemer MA (2014) Simulated global swell and wind-sea climate and their responses to anthropogenic climate change at the end of the twenty-first century. *J Clim* 27:3516–3536
- Gastineau G, Li L, Le Treut H (2009) The Hadley and Walker circulation changes in global warming conditions described by idealized atmospheric simulations. *J Clim* 22:3993–4013. <https://doi.org/10.1175/2009JCLI2794.1>
- Guo L, Perrie W, Long Z, Toulany B, Sheng J (2015) The impacts of climate change on the autumn North Atlantic wave climate. *Atmos Ocean* 53:491–509. <https://doi.org/10.1080/07055900.2015.1103697>
- Harris DL (1963) Characteristics of the hurricane storm surge. Tech Rep 48, US Weather Bureau, Department of Commerce, Washington, DC
- Hasselmann S, Brüning C, Hasselmann K, Heimbach P (1996) An improved algorithm for retrieval of ocean wave spectra

- from synthetic aperture radar image spectra. *J Geophys Res* 101:16615–16629
- Hemer MA, Trenham CE (2016) Evaluation of a CMIP5 derived dynamical global wind wave climate model ensemble. *Ocean Model* 103:190–203. <https://doi.org/10.1016/j.ocemo.d.2015.10.009>
- Hemer MA, Katzfey J, Trenham CE (2013a) Global dynamical projections of surface ocean wave climate for a future high greenhouse gas emission scenario. *Ocean Model* 70:221–245. <https://doi.org/10.1016/j.ocemod.2012.09.008>
- Hemer M, Fan Y, Mori N, Semedo A, Wang X (2013b) Projected changes in wave climate from a multi-model ensemble. *Nat Clim Change*. <https://doi.org/10.1038/nclimate1791>
- Hemer M, Wang W, Charles E, Hegermiller C & COWCLIP contributors (2014) Report of the 2014 meeting for the WCRP-JCOMM Coordinated Global Wave Climate Projections (COWCLIP), WMO 2014.
- Hemer M, Wang X, Webb A and COWCLIP contributors (2018) Report of the 2018 meeting for the WCRP-JCOMM Coordinated Global Wave Climate Projections (COWCLIP), WMO 2018
- Hersbach H et al (2020) The ERA5 global reanalysis. *Q J R Meteorol Soc*. <https://doi.org/10.1002/qj.3803>
- Johanson CM, Fu Q (2009) Hadley cell widening: model simulations versus observations. *J Clim* 22:2713–2725. <https://doi.org/10.1175/2008JCLI2620.1>
- Jullien S, Marchesiello P, Menkes CE, Lefèvre J, Jourdain NC, Samson G, Lengaigne M (2014) Ocean feedback to tropical cyclones: climatology and processes. *Clim Dyn* 43:2831–2854. <https://doi.org/10.1007/s00382-014-2096-6>
- Jury MR (2018) Characteristics and meteorology of Atlantic swells reaching the Caribbean. *J Coastal Res* 34:400–412. <https://doi.org/10.2112/JCOASTRES-D-17-00029.1>
- Kar-Man Chang E (2018) CMIP5 projected change in Northern Hemisphere winter cyclones with associated extreme winds. *J Clim* 31:6527–6542
- Kishimoto R, Shimura T, Mori N, Mase H (2017) Statistical modeling of global mean wave height considering principal component analysis of sea level pressures and its application to future wave height projection. *Hydrol Res Lett* 11:51–57. <https://doi.org/10.3178/HRL.11.51>
- Knapp KR, Kruk MC, Levinson DH, Diamond HJ, Neumann CJ (2010) The international best track archive for climate stewardship (IBTrACS): unifying tropical cyclone data. *Bull Am Meteorol Soc* 91:363–376. <https://doi.org/10.1175/2009BAMS2755.1>
- Komar PD (1998) Beach processes and sedimentation. Prentice-Hall, Upper Saddle River, NJ, 2nd edn. pp. 546, ISBN 0-13754-938-5
- Krien Y, Arnaud G, Cécé R, Ruf C, Belmadani A, Khan J, Bernard D, Islam AKMS, Durand F, Testut L, Palany P, Zahibo N (2018) Can we improve parametric cyclonic wind fields using recent satellite remote sensing data? *Remote Sens* 10:1963. <https://doi.org/10.3390/rs10121963>
- Laugel A, Menendez M, Benoit M, Mattarolo G, Méndez F (2014) Wave climate projections along the French coastline: dynamical versus statistical downscaling methods. *Ocean Model* 84:35–50. <https://doi.org/10.1016/j.ocemod.2014.09.002>
- Lemos G, Menendez M, Semedo A, Camus P, Hemer M, Dobrynin M, Miranda PMA (2020) On the need of bias correction methods for wave climate projections. *Glob Planet Chang* 186. <https://doi.org/10.1016/j.gloplacha.2019.103109>
- Moon I, Hara T, Ginis I, Belcher SE, Tolman HL (2004) Effect of surface waves on air-sea momentum exchange: I. Effect of mature and growing seas. *J Atmos Sci* 61(19):2321–2333
- Mori N, Yasuda T, Mase H, Tom T, Oku Y (2010) Projection of extreme wave climate change under global warming. *Hydrol Res Lett* 4:15–19. <https://doi.org/10.3178/HRL.4.15>
- Mori N, Shimura T, Yasuda T, Mase H (2013) Multi-model climate projections of ocean surface variables under different climate scenarios—future change of waves, sea level and wind. *Ocean Eng* 71:122–129. <https://doi.org/10.1016/j.oceaneng.2013.02.016>
- Morim J, Hemer M, Cartwright N, Strauss D, Andutta F (2018) On the concordance of 21st century wind-wave climate projections. *Global Planet Change* 167:160–171
- Morim J, Hemer M, Wang XL, Cartwright N, Trenham C, Semedo A, Young I, Bricheno L, Camus P, Casas-Prat M, Erikson L, Mentaschi L, Mori N, Shimura T, Timmermans B, Aarnes O, Breivik O, Behrens A, Dobrynin M, Menendez M, Staneva J, Wehner M, Wolf J, Kamranzad B, Webb A, Stopa J, Andutta F (2019) Robustness and uncertainties in global multivariate wind-wave climate projections. *Nat Clim Change*. <https://doi.org/10.1038/s41558-019-0542-5>
- Murakami H, Mizuta R, Shindo E (2012) Future changes in tropical cyclone activity projected by multi-physics and multi-SST ensemble experiments using the 60-km-mesh MRI-AGCM. *Clim Dyn* 39:2569–2584. <https://doi.org/10.1007/s00382-011-1223-x>
- Perez J, Menendez M, Losada IJ (2017) GOW2: a global wave hindcast for coastal applications. *Coastal Eng* 124:1–11. <https://doi.org/10.1016/j.coastaleng.2017.03.005>
- Piolle JF, Dodet G, Ash E (2020) ESA Sea State Climate Change Initiative: Product user guide, version 1.0. http://dap.ceda.ac.uk/thredds/fileServer/neodc/esacci/sea_state/docs/v1.1/Sea_State_cci_PUG_v1.0-signed.pdf. Accessed 21 Mar 2020
- Powell MD, Vickery PJ, Reinhold TA (2003) Reduced drag coefficient for high wind speeds in tropical cyclones. *Nature* 422(6929):279–283
- Rappaport EN (2014) Fatalities in the United States from Atlantic tropical cyclones: new data and interpretation. *Bull Am Meteorol Soc* 95:341–346. <https://doi.org/10.1175/BAMS-D-12-00074.1>
- Rayner NA, Parker DE, Horton EB, Folland CK, Alexander LV, Rowell DP, Kent EC, Kaplan A (2003) Global analyses of sea surface temperature, sea ice, and night marine air temperature since the late nineteenth century. *J Geophys Res* 108:4407. <https://doi.org/10.1029/2002JD002670>
- Rey T, Leone F, Candela T, Belmadani A, Palany P, Krien Y, Cécé R, Gherardi M, Péroche M, Zahibo N (2019) Coastal processes and influence on damage to urban structures during Hurricane Irma (St-Martin & St-Barthélemy, French West Indies). *J Mar Sci Eng* 7:215. <https://doi.org/10.3390/jmse7070215>
- Roberts MJ et al (2020a) Impact of model resolution on tropical cyclone simulation using the HighResMIP-PRIMAVERA multi-model ensemble. *J Clim* 33:2557–2583. <https://doi.org/10.1175/JCLI-D-19-0639.1>
- Roberts MJ et al (2020b) Projected future changes in tropical cyclones using the CMIP6 HighResMIP multi-model ensemble. *Geophys Res Lett* 47:e2020GL088662. <https://doi.org/10.1029/2020GL088662>
- Roehrig R et al (2020) The CNRM global atmosphere model ARPEGE-Climate 6.3: description and evaluation. *J Adv Model Earth Sys* 12:e2020MS002075. <https://doi.org/10.1029/2020MS002075>
- Soccimarro E, Gualdi S, Bellucci A, Sanna A, Fogli PG, Manzini E, Vichi M, Oddo P, Navarra A (2011) Effects of tropical cyclones on ocean heat transport in a high-resolution coupled general circulation model. *J Clim* 24:4368–4384. <https://doi.org/10.1175/2011jcli4104.1>
- Semedo A, Sušelj K, Rutgersson A, Sterl A (2011) A global view on the wind sea and swell climate and variability from ERA-40. *J Clim* 24:1461–1479. <https://doi.org/10.1175/2010JCLI3718.1>
- Semedo A, Weisse R, Behrens A, Sterl A, Bengtsson L, Günther H (2013) Projection of global wave climate change toward the end of the twenty-first century. *J Clim* 26:8269–8288. <https://doi.org/10.1175/JCLI-D-12-00658.1>

- Semedo A, Dobrynin M, Lemos G, Behrens A, Staneva J, De Vries H, Sterl A, Bidlot JR, Miranda PMA, Murawski J (2018) CMIP5-derived single-forcing, single-model, and single-scenario wind-wave climate ensemble: configuration and performance evaluation. *J Mar Sci Eng* 6:90. <https://doi.org/10.3390/jmse6030090>
- Shimura T, Mori N, Mase H (2015) Future projections of extreme ocean wave climates and the relation to tropical cyclones: ensemble experiments of MRI-AGCM3.2H. *J Clim* 28:9838–9856
- Stockdon HF, Holman RA, Howd PA, Sallenger AH (2006) Empirical parameterization of setup, swash, and runup. *Coastal Eng* 53:573–588
- Stockdon HF, Thompson DM, Plant NG, Long JW (2014) Evaluation of wave runup predictions from numerical and parametric models. *Coastal Eng* 92:1–11
- Stopa JE (2018) Wind forcing calibration and wave hindcast comparison using multiple reanalysis and merged satellite wind datasets. *Ocean Model* 127:55–69. <https://doi.org/10.1016/j.ocemo.2018.04.008>
- Timmermans B, Stone D, Wehner M, Krishnan H (2017) Impact of tropical cyclones on modeled extreme wind-wave climate. *Geophys Res Lett* 44:1393–1401. <https://doi.org/10.1002/2016GL071681>
- Timmermans BW, Gommenginger CP, Dodet G, Bidlot JR (2020) Global wave height trends and variability from new multimission satellite altimeter products, reanalyses, and wave buoys. *Geophys Res Lett* 47. <https://doi.org/10.1029/2019GL086880>
- Voltaire A et al (2019) Evaluation of CMIP6 DECK experiments with CNRM-CM6-1. *J Adv Model Earth Sys* 11(7):2177–2213
- Vousdoukas MI, Mentaschi L, Voukouvalas E, Verlaan M, Jevrejeva S, Jackson LP, Feyen L (2018a) Global probabilistic projections of extreme sea levels show intensification of coastal flood hazard. *Nat Comm* 9:2360. <https://doi.org/10.1038/s41467-018-04692-w>
- Vousdoukas MI, Mentaschi L, Voukouvalas E, Bianchi A, Dottori F, Feyen L (2018b) Climatic and socioeconomic controls of future coastal flood risk in Europe. *Nat Clim Change* 8:776–780. <https://doi.org/10.1038/s41558-018-0260-4>
- WAMDI Group (1988) The WAM model: a third-generation ocean wave prediction model. *J Phys Oceanogr* 18:1775–1810
- Wang XL, Feng Y, Swail VR (2014) Changes in global ocean wave heights as projected using multimodel CMIP5 simulations. *Geophys Res Lett* 41:1026–1034. <https://doi.org/10.1002/2013GL058650>
- Wang XL, Feng Y, Swail VR (2015) Climate change signal and uncertainty in CMIP5-based projections of global ocean surface wave heights. *J Geophys Res Oceans* 120:3859–3871. <https://doi.org/10.1002/2015JC010699>
- Webb A, Shimura T, Mori N (2018) A high-resolution future wave climate projection for the coastal northwestern Atlantic. *J Japan Soc Civil Eng, Ser B2 (Coastal Eng)* 74:1345–1350. https://doi.org/10.2208/kaigan.74.I_1345
- Wehner M, Prabhat RKA, Stone D, Collins WD, Bacmeister J (2015) Resolution dependence of future tropical cyclone projections of CAM5.1 in the U.S. CLIVAR hurricane working group idealized configurations. *J Clim* 28:3905–3925. <https://doi.org/10.1175/JCLI-D-14-00311.1>
- World Meteorological Organization (2014) Atlas of mortality and economic losses from weather, climate and water extremes (1970–2012). WMO-No. 1123
- Zelinsky DA (2019) Hurricane Lorenzo. Tropical Cyclone Report, National Hurricane Center, Miami, FL, USA. Available online: https://www.nhc.noaa.gov/data/tcr/AL132019_Lorenzo.pdf. Accessed 1 Jun 2020

Publisher's Note Springer Nature remains neutral with regard to jurisdictional claims in published maps and institutional affiliations.